



HAL
open science

Discrete Complex Analysis

Christian Mercat

► **To cite this version:**

Christian Mercat. Discrete Complex Analysis. Mathematics [math]. Université Montpellier II - Sciences et Techniques du Languedoc, 2009. tel-00439782

HAL Id: tel-00439782

<https://theses.hal.science/tel-00439782v1>

Submitted on 8 Dec 2009

HAL is a multi-disciplinary open access archive for the deposit and dissemination of scientific research documents, whether they are published or not. The documents may come from teaching and research institutions in France or abroad, or from public or private research centers.

L'archive ouverte pluridisciplinaire **HAL**, est destinée au dépôt et à la diffusion de documents scientifiques de niveau recherche, publiés ou non, émanant des établissements d'enseignement et de recherche français ou étrangers, des laboratoires publics ou privés.

HABILITATION À DIRIGER LES RECHERCHES EN SCIENCES

présentée à

L'UNIVERSITÉ DE MONTPELLIER 2

Spécialité

MATHÉMATIQUES

par

Christian MERCAT

Sujet du mémoire:

Analyse complexe discrète

présentée et soutenue publiquement le mercredi 9 décembre 2009 à Montpellier
devant le jury composé de

Pr. Vladimir MATVEEV (université de Bourgogne)	Président du jury et rapporteur
Pr. Jean-Marie MORVAN (université Claude Bernard, Lyon)	Rapporteur
Pr. Frank NIJHOFF (université de Leeds)	Rapporteur
Pr. Valérie BERTHÉ (université Montpellier 2)	Examinatrice
Pr. Rémy MALGOUYRES (université d'Auvergne)	Examineur
Pr. Jean-Pierre RÉVEILLÈS (université d'Auvergne)	Examineur

Contents

Curriculum Vitae	5
List of publications	7
Chapter 1. Presentation of scientific activity	9
1.1. Synthesis of work	9
1.1.1. Discrete Complex Analysis	9
1.1.2. Integrable Models	12
1.1.3. Exactly Solvable Models in Statistical Mechanics	15
1.1.4. Topology	16
1.2. PhD supervision	17
1.2.1. Diffusion processes	17
1.2.2. Discrete Laplacian	18
1.2.3. Digital Geometry	18
1.2.4. Fuzzy set	19
1.2.5. Discrete derivatives	21
Chapter 2. Discrete RIEMANN Surfaces	23
2.1. Conformal maps	23
2.2. Real discrete conformal structure	28
2.2.1. Graphs and Discrete Conformal Structure	28
2.2.2. Complexes	29
2.2.3. Averaging forms	30
2.2.4. HODGE star	31
2.2.5. Wedge product	31
2.2.6. Energies	32
2.2.7. Quasi-conformal maps	33
2.2.8. Abelian forms	34
2.2.9. Numerics with surfaces tiled by squares	35
2.2.10. Polyhedral surfaces	36
2.2.11. Towards a discrete RIEMANN-ROCH Theorem	38
2.3. Non real conformal structure	40
2.3.1. Complex HODGE star	40
2.3.2. Surfel surfaces	41
Chapter 3. Discrete Complex Analysis and Integrability	45
3.1. DARBOUX-BÄCKLUND transformation	46
3.2. Zero-curvature representation and isomonodromic solutions	47
3.3. Integrability and linear theory	48
3.3.1. Exponential	48

3.3.2. Integration	50
3.3.3. Isomonodromic solutions, the GREEN function	52
Chapter 4. Statistical Mechanics	55
4.1. The critical ISING model	55
4.1.1. BOLTZMANN law	55
4.1.2. The fermion ψ	56
4.2. The critical A - D - E models	57
4.2.1. A - D - E models	57
4.2.2. Graph fusion algebra	59
4.2.3. OCNEANU algebra	60
4.2.4. Critical A - D - E models	61
4.2.5. Fusion Projector	63
4.2.6. Fused face operators	64
Bibliography	67

Curriculum Vitae

Christian Mercat

I3M UMR 5149 Université Montpellier 2
Place Eugène Bataillon, c.c. 51
F-34095 Montpellier cedex 5
Maître de conférence

mercat@math.univ-montp2.fr

Phone: +33 4 67 14 42 33

Fax: +33 4 67 14 35 58

http://www.math.univ-montp2.fr/SPIP/_MERCAT-Christian_

married, born July 3rd 1969

Diplomas

- 1998 PhD thesis at the Louis Pasteur University (Strasbourg),
under supervision of Daniel BENNEQUIN
- 1996 Agrégation de Mathématiques
- 1993 Magistère de l'École Normale Supérieure de Paris (M.Sc.)
- 1992 Diplôme d'Étude Approfondie (Strasbourg)
- 1990-95 École Normale Supérieure de Paris

Professional Experience

- Sept. 2003- Maître de conférences (associate professor) at the Montpellier 2 University
- 2002-2003 Postdoc at the Technical University Berlin
- 2000-2001 Postdoc at the University of Melbourne
- Sep.-Dec. 1999 Professeur agrégé, Champlain highschool, Chennevière/M.
- Jan.-Aug. 1999 Postdoc at the Tel Aviv University, Israel
- Sep.-Dec. 1998 Postdoc at the MITTAG-LEFFLER Institute, Sweden

Other Activities

- 2008- PhD supervision of Frédéric RIEUX on digital diffusion and convolution
applied to discrete analysis
 - 2006- 2008 3 M.Sc. in computer science supervisions.
 - 2008- Member of the Directing Committee of the Pôle MIPS (Mathematics,
Computer Sc., Physics, Mechanics) of the University Montpellier 2
 - 2007- Initiator of the Inter2Geo European project
 - 2009- Partner of the Math-Bridge European project
- Reviewer for SIGGRAPH, ACM Trans. On Graph., IWCIA, Duke Math. J.,
Adv. Appl. Math., J. of Math. Ph., Eur. Phys. J., J. Diff. Eq. Appl.,
L. in Math. Ph.; 15 reviews in MathSciNet.
- Languages: French (native), English (fluent), German and Spanish (conversation)
- Computer: Java, C++, python, PHP, MySQL, html, javascript, spip, joomla, xwiki,
mathematica, maple

List of publications

- [1] **B** Alexander Bobenko, Christian Mercat, and Markus Schmies. Conformal structures and period matrices of polyhedral surfaces. In A. Bobenko and Ch. Klein, editors, *Riemann Surfaces - Computational Approaches*, pages 1–13. 2009.
- [2] **C** Ulrich Kortenkamp, Christian Dohrmann, Yves Kreis, Carole Dording, Paul Libbrecht, and Christian Mercat. Using the Intergeo Platform for Teaching and Research. The Ninth International Conference on Technology in Mathematics Teaching (ICTMT 9), Metz, France, July 6-9 (2009).
- [3] **V** Applications conformes. *Images des mathématiques*, Mar. 2009. <http://images.math.cnrs.fr/Applications-conformes.html>.
- [4] **C** Ulrich Kortenkamp, Axel M. Blessing, Christian Dohrmann, Yves Kreis, Paul Libbrecht, and Christian Mercat. Interoperable interactive geometry for europe - first technological and educational results and future challenges of the intergeo project. CERME 6 - Sixth Conference of European Research in Mathematics Education, Lyon, France, Jan. 28-Feb 1 (2009).
- [5] **V** De beaux entrelacs. *Images des mathématiques*, Feb. 2009. <http://images.math.cnrs.fr/De-beaux-entrelacs.html>.
- [6] **C** Discrete complex structure on surfel surfaces. Coeurjolly, David (ed.) et al., Discrete geometry for computer imagery. 14th IAPR international conference, DGCI 2008, Lyon, France, April 16–18, 2008. Proceedings. Berlin: Springer. Lecture Notes in Computer Science 4992, 153-164 (2008)., 2008.
- [7] **C** Paul Libbrecht, Cyrille Desmoulin, Ch. M., Colette Laborde, Michael Dietrich, and Maxim Hendriks. Cross-curriculum search for Intergeo. Autexier, Serge (ed.) et al., Intelligent computer mathematics. 9th international conference, AISC 2008, 15th symposium, Calculemus 2008, 7th international conference, MKM 2008, Birmingham, UK, July 28–August 1, 2008. Proceedings. Berlin: Springer. Lecture Notes in Computer Science 5144. Lecture Notes in Artificial Intelligence, 520-535 (2008)., 2008.
- [8] **B** Discrete riemann surfaces. In Athanase Papadopoulos, editor, *Handbook of Teichmüller Theory, vol. I*, volume 11 of *IRMA Lect. Math. Theor. Phys.*, pages 541–575. Eur. Math. Soc., Zürich, 2007.
- [9] **V** Keltische Flechtwerke. *Spektrum der Wissenschaft*, Special issue Ethnomathematik:46–51, Nov. 2006. <http://www.spektrum.de/artikel/856963>.
- [10] **A** Alexander I. Bobenko, Ch. M., and Yuri B. Suris. Linear and nonlinear theories of discrete analytic functions. Integrable structure and isomonodromic Green’s function. *J. Reine Angew. Math.*, 583:117–161, 2005.
- [11] **A** Exponentials form a basis of discrete holomorphic functions on a compact. *Bull. Soc. Math. France*, 132(2):305–326, 2004.
- [12] **A** C. H. O. Chui, Ch. M., and Paul A. Pearce. Integrable and conformal twisted boundary conditions for $sl(2)$ A - D - E lattice models. *J. Phys. A*, 36(11):2623–2662, 2003.
- [13] **B** C. H. Otto Chui, Ch. M., and Paul A. Pearce. Integrable boundaries and universal TBA functional equations. In *MathPhys odyssey, 2001*, volume 23 of *Prog. Math. Phys.*, pages 391–413. Birkhäuser Boston, Boston, MA, 2002.
- [14] **A** C. H. Otto Chui, Ch. M., William P. Orrick, and Paul A. Pearce. Integrable lattice realizations of conformal twisted boundary conditions. *Phys. Lett. B*, 517(3-4):429–435, 2001.
- [15] **A** Ch. M. and Paul A. Pearce. Integrable and conformal boundary conditions for Z_k parafermions on a cylinder. *J. Phys. A*, 34(29):5751–5771, 2001.

- [16] **A** Discrete Riemann surfaces and the Ising model. *Comm. Math. Phys.*, 218(1):177–216, 2001.
- [17] **T** Holomorphie discrète et modèle d’Ising. PhD thesis, Université Louis Pasteur, Strasbourg, France, 1998. under the direction of Daniel Bennequin, Prépublication de l’IRMA, available at <http://www-irma.u-strasbg.fr/irma/publications/1998/98014.shtml>.
- [18] **V** Les entrelacs des enluminures celtes. *Pour la Science*, (Numéro Spécial Avril), 1997. www.entrelacs.net.
- [19] **V** Théorie des nœuds et enluminure celte. *l’Ouvert*, Num. 84:1–22, 1996, IREM de Strasbourg.

- A** Peer reviewed article
- B** Peer reviewed book chapter
- C** Peer reviewed conference proceeding
- T** PhD Thesis
- V** Non peer reviewed vulgarization

Presentation of scientific activity

1.1. Synthesis of work

In this section, I will summarise my scientific work, going backwards in time, without going into too many details, the following chapters being more comprehensive.

My present interest is in Discrete Differential Geometry, especially applied to Computer Graphics, but it stems from Discrete Complex Analysis and Integrable Models, which has been my main subject of study during the past 6 years. The intention is to translate the best part of the theory of surfaces and complex analysis to the era of computers and discrete surfaces. This XIXth century theory, paved the way to the world of engineering marvels of the XXth century. Its discrete counterpart would be a real benefit for many different subjects of industrial interest.

I have developed the theory of Discrete Complex Analysis and Discrete RIEMANN Surfaces as a tool to tackle issues in Exactly Solvable Models in Statistical Mechanics. The main idea is to try to see, in an exactly solvable model, a Finite Conformal Field Theory, without having to go to the thermodynamic limit. This life long project, set by my advisor Daniel BENNEQUIN, was given positive partial answers in my PhD thesis: criticality in the Ising model can be seen at the finite level as compatibility with discrete conformality.

1.1.1. Discrete Complex Analysis. This subject is at the heart of my work and most of my recent papers deal with it [6, 8, 10, 11]. The initial impulse, based on previous work by LELONG-FERRAND [62] and DUFFIN [59, 60], was given in my PhD thesis, summarized in Comm. in Math. Phys. [16, 17].

Analytic functions are everywhere, behind every key of hand-held calculators, like $x \mapsto x^2$, $1/x$, \tan , \exp , \log , and the theory of RIEMANN surfaces that generalizes them on non flat surfaces has proven to be a highlight of XIXth century mathematics. Nowadays, Computer Graphics use it to globally parameterize discrete surfaces for a variety of reasons, texture mapping, segmentation, remeshing, animation...

At the root of RIEMANN surfaces is the concept of complex differentiability and line integration of complex valued functions. In order to discretize these notions, one needs a discrete version of exterior differential calculus, HODGE theory and CAUCHY-RIEMANN equation.

Points in the Cartesian plane $(x, y) \in \mathbf{R}^2$ gain in being seen as complex numbers $x + iy \in \mathbf{C}$ with the famous “imaginary” number i such that $i^2 = -1$. But the XVIth century trick, of manipulating the square root of negative numbers, is now as “real” as the real line of lengths, giving to the complex numbers the structure of a field, with addition and multiplication, unifying points of the plane and Euclidean transformations of them: $\zeta \in \mathbf{C}$ is whether a point, a vector acting by translation

when added, or a similitude when multiplied. The similitude $z \mapsto \alpha z + \beta$ scales the whole plane by a factor $|\alpha|$ and turns it by an angle $\arg(\alpha)$.

A holomorphic function f is a complex differentiable function, that is a transformation of the plane which is, except at isolated critical points, *locally* a similitude and the local similitude factor is called the *derivative* f' of the function:

$$f(z + z_0) = f(z_0) + f'(z_0) \times z + o(z).$$

At the zero of the derivative, the function behaves locally like a monomial $z \mapsto z^k$. GOURSAT noticed that simply asking for this local feature of differentiability

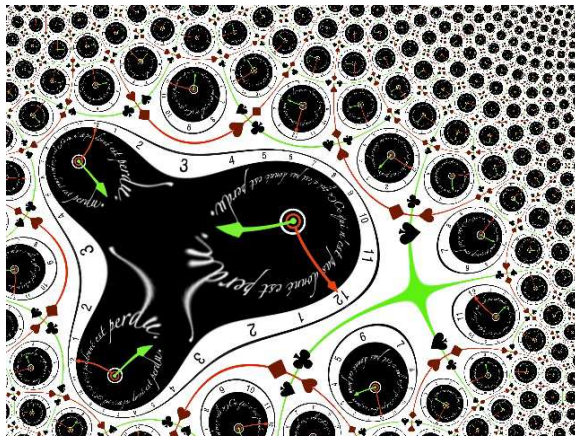


Figure 1.1: The pull-back of the picture of a clock paving the complex plane, by a polynomial (see Sec. 2.1). One can see the branchings at the zeros of the derivative where the zoom factor diverges.

actually implies that the derivative f' is itself a holomorphic function. Compared to the vast zoo of differentiable real functions, complex differentiation is very rigid.

A natural discretization of these equations takes place on cellular decompositions of surfaces by *quadrilaterals* of a given shape, the two dual diagonals locally playing the role of coordinates. With $\diamond_0, \diamond_1, \diamond_2$ the vertices, edges and faces of a quad-decomposition, for each face $(x, y, x', y') \in \diamond_2$ (see Fig. 1.2), prescribe a certain *diagonal ratio* ρ on the unoriented edges:

$$\rho(x, x') = \frac{1}{\rho(y, y')} = -i \frac{Z(y') - Z(y)}{Z(x') - Z(x)}$$

for any realization Z of the shape of the associated (oriented) quadrilateral in the complex plane. This ratio is by construction invariant by similitudes. It is real when diagonals are orthogonal (see Fig. 1.3). A function f on the vertices is said to be discrete holomorphic if, for each such face, the diagonal ratio of the image is unchanged:

$$f(y') - f(y) = i\rho(x, x')(f(x') - f(x)).$$

This equation is reminiscent of the CAUCHY-RIEMANN equation when the diagonals are orthogonal, mimicking local orthogonal coordinates and the compatibility between the partial derivatives.

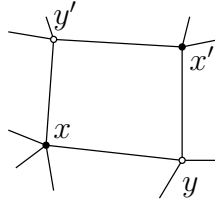


Figure 1.2: A quadrilateral (x, y, x', y') with a given shape in the complex plane.

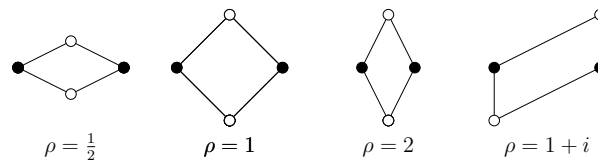


Figure 1.3: Different quadrilateral shapes and the associated diagonal ratio.

Although very simple, this definition yields a lot of results similar to the continuous theories of complex analysis and RIEMANN surfaces.

As in the continuous, there is a (infinitesimal) contour integration formula for the differentiation, analogous to $f'(z_0) = \lim_{\gamma \rightarrow z_0} \frac{i}{2\mathcal{A}(\gamma)} \oint_{\gamma} f(z) d\bar{z}$:

$$f'(x, y, x', y') := \oint_{\partial(x, y, x', y')} f(z) d\bar{z},$$

but it is only in the case of flat rhombi decompositions that the derivative itself can be integrated into a holomorphic function. A contour integral formula with a CAUCHY kernel holds as well for the value of a holomorphic function at an interior point given by its boundary values. This kernel is associated with the GREEN potential of the discrete LAPLACE operator, giving a discrete analogous of the logarithm. Every discrete holomorphic function is harmonic for this Laplacian and a discrete HODGE decomposition theorem splits forms into exact, co-exact and harmonic parts, the harmonic themselves in holomorphic and anti-holomorphic parts. In the flat rhombic case, we recovered in [10], using methods from integrable models, the result by KENYON [71] that gives an explicit formula for the discrete GREEN function.

The integration of functions is defined through a discrete wedge product that couples k and ℓ -forms into $k + \ell$ -forms. This is not trivial since functions, 1-forms and 2-forms don't live at the same place, respectively on vertices, edges and faces but averaging values on incident cells yields a consistent discrete exterior calculus fulfilling the expected LEIBNIZ rule $d(\alpha \wedge \beta) = d\alpha \wedge \beta + \alpha \wedge d\beta$. In the flat rhombic case, this product becomes compatible with holomorphy in the sense that holomorphic functions can be integrated into holomorphic functions, whereas in general, even though f is a holomorphic function and dZ a holomorphic 1-form,

the 1-form $f dZ$ is closed (that's the discrete CAUCHY's integral theorem) but not holomorphic.

Other authors investigated similar theories, especially DYNNIKOV and NOVIKOV [61] on the triangle lattice, and KISELMAN [74] in the framework of *monodriffic* functions.

1.1.2. Integrable Models. Holomorphy condition can be understood in terms of dynamical systems; indeed, there exists a GREEN potential for discrete holomorphic functions, the discrete GAUSS kernel $\frac{dz}{z-z_0}$, that allows to solve for a solution in the interior of a domain, given boundary values.

This is the point of view I took during my postdoctoral stay at the Technical University in Berlin, in the team of Alexander BOBENKO, where many constraints that define classes of surfaces, such as constant mean curvature surfaces, isothermic surfaces and so on, are treated in this way [38, 40, 66, 67, 68, 69].

The linear theory of Discrete Complex Analysis appeared to be the ground level in a hierarchy of discrete integrable models, called the ADLER, BOBENKO and SURIS hierarchy [20]. The actual first step is the so called $Q_1 \delta = 0$ equation of *preservation of cross-ratio* and can as well be understood as a model for discrete complex analysis:

Similarly to the linear case, fixing on each face $(x, y, x', y') \in \diamond_2$, a complex number $q(x, x') = \frac{1}{q(y, y')}$ allows to define a function f of the vertices to be *quadratic holomorphic* if, on each face, the cross-ratio of the four values is the fixed number:

$$\frac{f(y) - f(x)}{f(x) - f(y')} \frac{f(y') - f(x')}{f(x') - f(y)} = q(x, x').$$

Whereas the diagonal ratio of a quadrilateral is invariant under similitudes, the cross-ratio of its four vertices is invariant under the larger group of MÖBIUS transformations and while a holomorphic function is to the first order a similitude (away from zeros of its derivative), it is such a MÖBIUS transformation up to the second order:

$$f(z + z_0) = \frac{az + b}{cz + d} + o(z^2).$$

The condition of cross-ratio preservation can actually be unified with the linear version of diagonal ratio preservation because both can be seen as a discrete MORERA theorem: a function of the vertices is discrete holomorphic whenever

$$\oint_{\gamma} f dZ = 0$$

on every trivial loop γ . The difference between the linear and the quadratic version being the wedge product coupling functions to 1-forms; it is the *arithmetic* mean for the linear version, $\int_{(x,y)} f dZ := \frac{f(x)+f(y)}{2} \int_{(x,y)} dZ$, and the *geometric* mean for the quadratic one, $\int_{(x,y)} f dZ := \sqrt{f(x)f(y)} \int_{(x,y)} dZ$.

This is seen after a HIROTA change of variables: F is a map with the same cross-ratio as a map Z if and only if one can find a function f such that, on each edge $(x, y) \in \diamond_1$,

$$(1.1) \quad F(y) - F(x) = f(x) \times f(y) \times (Z(y) - Z(x)).$$

In effect, this transformation is a *derivation*, $dF = f dZ$ where the derivative (or, better, its square root, or its real and imaginary parts) f is split onto the two dual graphs. The cross-ratios of a function F verifying (1.1) is clearly the same as Z since the contributions of f cancel. The constraint on f is that the associated exact 1-form is actually closed: $\oint_{\partial(x,y,x',y')} f dZ = 0$.

After this change of variables, the linear theory can be shown to be a *linearization* of this quadratic theory around the trivial solution $f \equiv 1$.

We will see that *circle patterns* are special cross-ratio preserving maps where, the values for the derivative on the primal graph, center of circles, stay real, controlling the homothetic factor of the image circle, and the values on the dual graph stay unitary, controlling the rotational part of the local similitude. A linear discrete holomorphic function, real on the primal graph and pure imaginary on its dual, can be seen as an infinitesimal direction in the space of circle patterns. A geometric condition on circle patterns can be translated into a vector field of linear holomorphic functions pointing a direction of change. Such a vector field can be numerically integrated into a flow of circle patterns, converging to the desired circle pattern; I have done so in an applet using the Oorange development environment.

Both theories are, in some special configurations, *discrete integrable*, in the sense that some over-determinate problems have a solution, allowing for the construction of families of solutions and deformations of existing solutions:

The discrete conformal structure, that is to say the ratio ρ or q put on diagonals, can be defined by quantities that naturally live on the edges of the quadrilaterals, to be understood as the local directions of the quad-edge for a particular holomorphic map. We showed in [10] that the system is *integrable* when these quantities are constant along the directions attached to *train-tracks* [11, 72]: two edges belonging to the same train-track when they are opposite in a quadrilateral, like the two edges tagged α in Fig. 1.4.

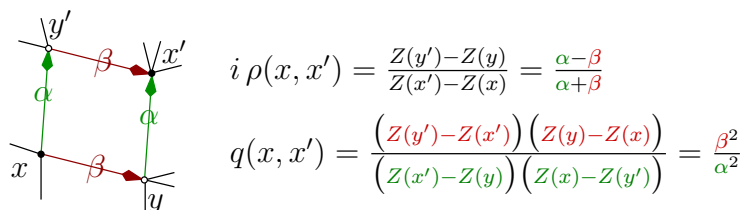


Figure 1.4: In the integrable case, the diagonal-ratio $\rho(x, x')$ and cross-ratio $q(x, x')$ depend on the edges of the quadrilateral.

Geometrically, it means that there exists a holomorphic map such that all faces are sent to *parallelograms*.

Integrability means that the system is *3D-consistent* [20, 10]:

PROPOSITION 1.1.1. *Consider a cube $(x, y_1, y_2, y_3, x_1, x_2, x_3, y)$ with opposite faces holding the same discrete conformal structure ratios and the system, which given four values $f(x), f(y_1), f(y_2), f(y_3)$, solves for the four values $f(x_1), f(x_2), f(x_3)$ and $f(y)$, with f a discrete holomorphic function (in the linear or quadratic framework). The system accepts a non trivial solution for $f(y)$ if and only if the discrete conformal structure comes from parallelograms.*

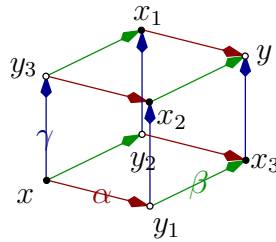


Figure 1.5: The four values $f(x), f(y_1), f(y_2), f(y_3)$ determine uniquely $f(x_1), f(x_2), f(x_3)$ when f is discrete holomorphic, but $f(y)$ is over-determined unless the weights come from parallelograms.

In this integrable case, the machinery of integrable systems gives us powerful tools, a zero curvature representation, DARBOUX-BÄCKLUND transformations and isomonodromic solutions.

Our main results in this respect was to unify the linear and quadratic cases in the same framework, and to recover KENYON's result [71] giving the GREEN function of the discrete Laplacian in the rhombic case as a linear combination of discrete exponential functions. We understood this GREEN function as an isomonodromic solution and gave interesting properties of the discrete exponential functions [10].

When the diagonal ratios ρ are *real* numbers, or the cross-ratios q are *unitary* numbers, it implies that these quadrilaterals are rhombi, where even more interesting features appear: primitives of holomorphic functions can be defined.

This *real* integrability condition has been singled out by DUFFIN [60] in the context of discrete complex analysis, and by BAXTER [30] as Z-invariant ISING model [24, 25, 42, 95].

In my thesis, I called this configuration *critical* for this link with exactly solvable models and Richard KENYON called it *isoradial* for its link with circle patterns [71, 55].

Notice that BAZHANOV, MANGAZEEV and SERGEEV make a connection between the ISING model and circle patterns in [32].

The cross-ratio preserving maps are closely related to the circle patterns idea [36, 98, 73, 43]. In this framework, proposed by THURSTON, a discrete conformal structure is defined by a pattern of intersecting circles. A holomorphic function is defined by another circle pattern of the same combinatorics such that a pair of intersecting circles is mapped to another pair of circles, intersecting at the same angle. A quadrilateral is defined for such a pair, defined by the two centers and the two points of intersection. The cross-ratio of these four points is given by the intersection angle. Therefore circle patterns is a special case of cross-ratio preserving maps. Circle packings are a limit case of circle patterns with tangential adjacencies. In circle pattern theory, the discrete conformal parameters come from *kite* quadrilaterals, with orthogonal diagonals. Integrability meaning parallelism of opposite sides is then associated with *rhombic* embedding, that is to say *isoradial* circle patterns. This way, a dual isoradial circle pattern emerges from the intersection points of the primal circle pattern, associated with the inverse cross-ratios.

Another way to view the 3D-consistency condition is to split the cube in two hexagons, the compatibility conditions are the same in both cases, see Fig. 1.8.

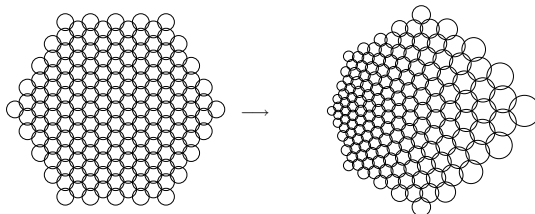


Figure 1.6: Pairs of patterns of intersecting circles are a discrete conformal map when the intersection angles are pair-wise preserved.

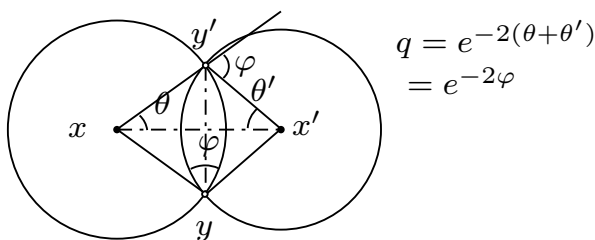


Figure 1.7: The cross-ratio of the centers and intersection points of two circles is given by their intersection angle.

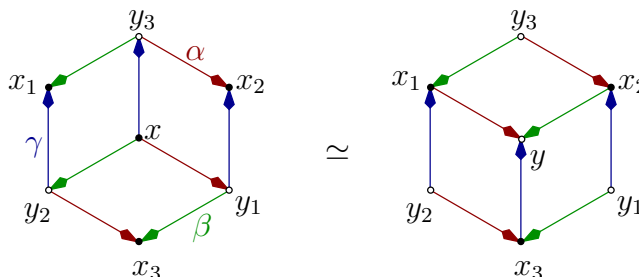


Figure 1.8: The six values $f(x_1), f(x_2), f(x_3), f(y_1), f(y_2), f(y_3)$ over-determine the values $f(x)$ and $f(y)$ for f a discrete holomorphic function. The compatibility conditions on these six values are the same in both cases if and only if the discrete conformal structure comes from parallelogram sides α, β, γ .

1.1.3. Exactly Solvable Models in Statistical Mechanics. The notion of integrability has several related meanings depending on the context. In statistical mechanics, it means that a thermodynamic continuous limit can be taken and it usually comes from a YANG-BAXTER equation. A finer notion is *criticality* where this continuous limit is special, exhibiting a phase transition. In exactly solvable models, interesting critical systems, like the ISING model or its *A-D-E* -generalizations [47, 86], have a *conformal* continuous limit, in particular some 2-point correlation functions decay not exponentially fast with the distance between

the two points but as a power law (see LANGLANDS, LEWIS and ST AUBIN [76]). More generally, an observable depends not on the detail of the surface with marked points but more specifically on its conformal class. It was a goal of my PhD advisor Daniel BENNEQUIN to find in the discrete setup of critical models what remained of BELAVIN, POLYAKOV and ZAMOLODCHIKOV *conformal blocks*.

I made advances in this program for the ISING model: I proved in my thesis [16, 17] that the geometric condition of (real) integrability, already singled out by BAXTER as Z -invariant ISING model [31], pinpointed the fact that a special observable in the ISING model, the fermion $\psi_{x,y}$, became a discrete DIRAC spinor, a discrete holomorphic analog of \sqrt{dz} . This is why I named this configuration *critical*.

In Australia, in collaboration with Paul A. PEARCE, I investigated other statistical models, with the view to try and understand them in the framework of discrete RIEMANN surfaces [12, 13, 14, 15]. We identified the integrable conformal twisted boundary conditions, on surfaces with boundary or as seams inserted in a closed surface along a loop, in several exactly solvable statistical models. We begun with the parafermions Z_k [15], we investigated the relation between such twisted boundary conditions in conformal field theory [90, 89, 91, 51] and their lattice realization for A - D - E models [14], and understood it in the framework of the Thermodynamic BETHE-ANSATZ [13]. We entangled in the fusion procedure the contribution of different nodes in the OCNEANU graph [85] and clarified a correspondence between the nodes of the OCNEANU graphs and our twisted discrete seams [12], ending up with a discrete version of the Vertex Operator Algebra governing the fusion rules.

Unfortunately, I didn't succeed in making the connection between chirality, present in our twisted conformal boundary conditions, and discrete holomorphic/antiholomorphic conformal blocks. What I missed was a clearer notion of discrete fiber bundle, more elaborate than the simple double-cover of spinors that I constructed by hand. I saw that the parafermion theory would have worked in a similar way but didn't pursue in this direction, having enough on my hands with the development of the theory of discrete RIEMANN surfaces in the framework of Discrete Differential Geometry. And what begun as a tool to tackle a problem in statistical mechanics ended up being my primary object of study.

Other researchers, independently or not, picked up similar ideas and discrete holomorphic functions theory was applied to statistical mechanics, by COSTA-SANTOS and MCCOY [53, 54] for higher genus ISING and dimer models, by RAJABPOUR and CARDY [93] for discrete holomorphic parafermions, DE TILIÈRE and BOUTILLIER [41, 42] for the Z -invariant ISING model and dimers, and SMIRNOV and CHELKAK [102, 103, 48] for conformal invariance of percolation and more generally in 2D lattice models, making the link with hard-core probability theory like loop-erased random walks [77].

1.1.4. Topology. Our interest for a discrete version of conformal blocks takes its root in topology: The VERLINDE formula governs the compatibility of the dimensions of these blocks under fusion rules. This essentially finite information can be used to build topological invariants like knots invariants. Daniel BENNEQUIN idea was that a discrete version of conformal blocks for statistical mechanics would have saved the trouble to go, from an exactly solvable model, to a conformal theory, back to the discrete data of its fusion rules [33].

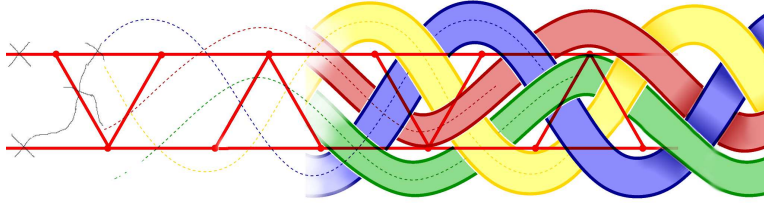


Figure 1.9: A 1-1-correspondence between edge signed planar graphs and regular projections of links helps to manipulate and beautifully draw knots.

This interest in low dimensional topology came from my Diploma, conducted by Daniel BENNEQUIN, in Strasbourg, where I showed the equivalence between SINGER theorem on HEEGAARD diagrams and KIRBY theorem on DEHN surgeries.

This led to a long lasting interest in knot theory and its popularization, with (non peer reviewed) articles in the press [5, 9, 18, 19], with conferences addressed to the general public, specialized courses to draw nice knots and a popular website <http://entrelacs.net> (see Fig. 1.9).

1.2. PhD supervision

I am co-advising the thesis of Frédéric RIEUX, together with Pr Christophe FIORIO. Frédéric is beginning his second year and I am going to summarize the goals of his thesis and his first promising results.

The main goal is to be able to recognize a set of points in an \mathbf{R}^n as a discretization of a manifold. Our idea is to define a diffusion process and analyze it, in order to guess the correct dimension by the diffusion speed, and local geometry. Once this identification is done, we use the local homogeneous coordinates to discretize usual differential geometry and perform discrete analysis, derivation with estimation of tangents, of curvature, and so on.

1.2.1. Diffusion processes. Heat kernel or random walks have been widely used in image processing, for example lately by SUN, OVSJANIKOV and GUIBAS [105] and GEBAL, BÆRENTZEN, AANÆS and LARSEN [63] in shape analysis. It is indeed a very precious tool because two manifolds are isometric if and only if their heat kernels are the same (in the non degenerate case).

The heat kernel k_t of a manifold M maps a couple of points $(x, y) \in M \times M$ to a positive real number $k_t(x, y)$ which describes the transfer of heat from y to x in time t . Starting from a (real) temperature T on M , the temperature after a time t at a point x is given by

$$H^t f(x) = \int_M f(y) k_t(x, y) dy.$$

The distance can be recovered from the heat kernel:

$$d_M^2(x, y) = -4 \lim_{t \rightarrow 0} t \log k_t(x, y).$$

The heat equation drives the diffusion process, the evolution of the temperature in time is governed by the (spatial) LAPLACE-BELTRAMI operator Δ_M :

$$\frac{\partial f(t, x)}{\partial t} = -\Delta_M f(t, x).$$

It implies that if the eigenvalues of the Laplacian are $\text{sp}(\Delta_M) = \{\lambda_i\}_{i \in \mathbf{N}}$, associated with eigenvector functions ϕ_i , then the heat kernel is

$$k_t(x, y) = \sum_i e^{-\lambda_i t} \phi_i(x) \phi_i(y).$$

1.2.2. Discrete Laplacian. The first issue to use these ideas in the discrete setup is to define a good discrete Laplacian, or equivalently, a good diffusion process. This diffusion process should be reasonably robust to noise, to outliers (points which are added by mistake) and to missing data.

This situation is understood in the realm of polyhedral surfaces and triangulations, and a time appraised discrete Laplacian, based on sound theoretical grounds is known for a long time, the so-called *cotangent weights* Laplacian [92], which is the same as the one we talked about in the framework of discrete RIEMANN surfaces:

$$\Delta f(x) = \sum_{(x, x_i) \in \Gamma_1} \rho(x, x_i) (f(x_i) - f(x))$$

$$\text{where } \rho(x, x_i) = \frac{1}{2} (\cotan \widehat{x_i x_{i-1} x} + \cotan \widehat{x x_{i+1} x_i}) = \frac{d(y_{i+1}, y_i)}{d(x_i, x)}$$

with the triangle angles, the intrinsic metric computed on the flattened triangles pair and y_i the center of the circumcircle to the triangle (x_i, x, x_{i-1}) , similarly for y_{i+1} , as depicted in Fig. 1.10.

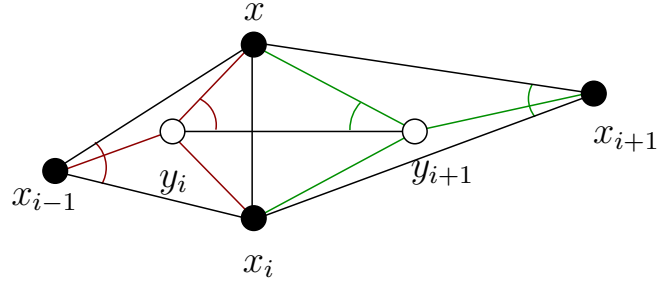


Figure 1.10: The diagonal ratio $\frac{d(y_{i+1}, y_i)}{d(x_i, x)}$ is the mean of the cotangents of the angles at x_{i-1} and x_{i+1} .

1.2.3. Digital Geometry. But the situation in Digital Geometry is somehow different, the data that is produced by a 3D-scanner is composed of a set of voxels (cubes in \mathbf{Z}^3) that samples the underlying continuous object. How can a good diffusion process be defined on such a locally rigid geometry?

We first studied a random walk based on the celebrated short-sighted drunkard's walk, with equiprobability, no memory and no long range decision, the walker goes from a voxel cube, equiprobably to one of its 2^d vertices, and then equiprobably to one of the available voxel of the object adjacent to it.

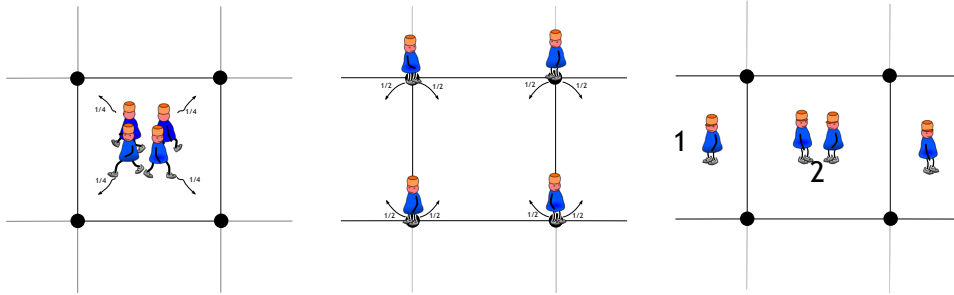


Figure 1.11: 2^n walkers on a line in \mathbf{Z}^2 recover the binomials $\binom{n}{p}$.



Figure 1.12: There are only four local masks appearing on an 8-connected line in the first octant.

We began with a discrete curve in \mathbf{Z}^2 . We showed that for this process on a discrete line [94], the probability to find the walker at a certain point y , at a (discrete) time t , having begun at x is equivalent (for large t) to a normal distribution $\frac{1}{\sqrt{2\pi\sigma}} e^{-d(x,y)^2/2\sigma^2}$ with the dispersion $\sigma(t)$ increasing over time (proportional to \sqrt{t}). It is a direct application of the Central Limit Theorem, our process being ergodic and similar patterns being repeated with a well defined probability. The same kind of argument will work in any dimension.

Unfortunately this dispersion depends on the *slope* of the line because 8-connected pixels act as bottle-necks compared to 4-connected pixels (see Fig.1.13).

1.2.4. Fuzzy set. Conductivity in crystals led me to think about *tunnel effect* transition in quantum mechanics, where electrons can leap from a conductor to another. So we naively tried a *fuzzy* transition, allowing walkers to wander one step away from the discrete line, on a thickened line with ghost pixels, in the 4-connected or 8-connected directions, projecting them back, later on, to the underlying line (see Fig. 1.14). This fuzzy diffusion is slower than the original one.

We have two parameters to play with, the allowed probabilities associated with 4 and 8 new neighbors. We optimized these probabilities in order to have a minimum deviation among the deviations for different slopes. This minimum is reached when 4 and 8-connected ghost pixels are both half as probable as the genuine pixels.

So beginning from a set of pixels, we add its 4 and 8-connected neighbors, with decreased probability, setup our random walk, and read from the weights of this process the adaptive distances between our points and integrate it into a curvilinear abscissa on our set.

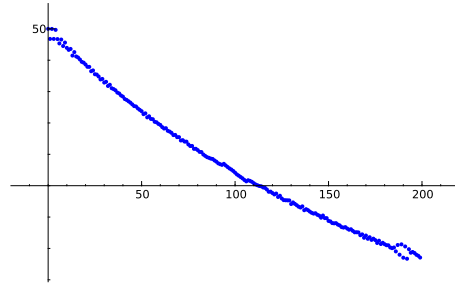


Figure 1.13: Deviations of a typical mask on two hundred discrete lines of increasing slopes in the first octant. The minimum is reached for lines of slope 1 with only 8-connected pixels.

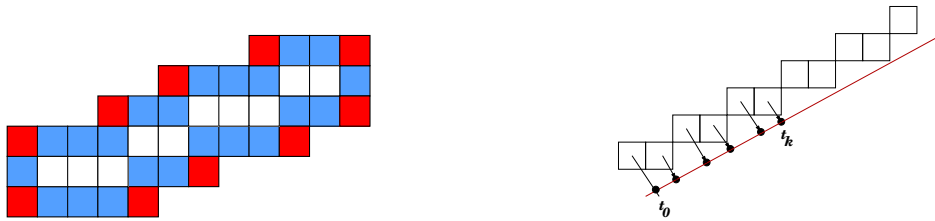


Figure 1.14: Fuzzy segment with *ghost* 4 and 8 - connected pixels, which are projected onto the underlying line.

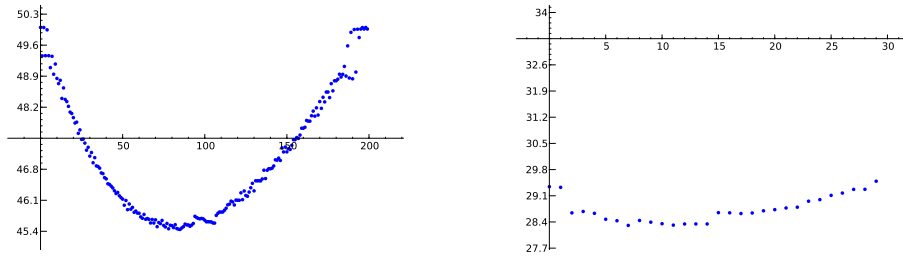


Figure 1.15: Deviations for different lines using the curvilinear abscissa on the thin line and on the fuzzy line for optimized parameters.

The optimization procedure is there to insure that this process, when done on discrete lines, end up with what we should expect, that is to say a normal law with respect to the Euclidean distance in \mathbf{R}^2 . So if the set is modeled on a curve, with feature size much lower than the size of discretization, a size of averaging mask large enough but lower than this feature size should recover the local geometry of the curve.

In order to denoise a function defined on the set, we simply convolve it with a certain power of the diffusion process. This power can be adaptive: large in flat

areas and small in tormented areas with small local feature size. The diffusion could be as well tailored in order to be non symmetric near sharp features to be preserved.

1.2.5. Discrete derivatives. Once this diffusion mask is defined, we use it to do numerical analysis on digital curves, computing derivative of functions such as tangency and curvature.

Consider the connected discretized graph of a function as a discrete curve in \mathbf{Z}^2 . By applying the previous method, we are able to compute derivatives of this function by applying discrete derivative masks and convolving with our averaging kernel with a remarkable accuracy, as illustrated in Fig. 1.16 and 1.17.

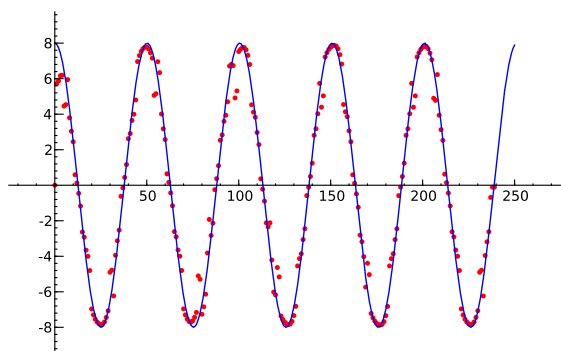


Figure 1.16: Estimation of the discrete adaptive derivative function of $x \mapsto \sin(x)$ and the values of the real derivative function $x \mapsto \cos(x)$, computed according to a mask of length 15 on a sample of 250 points.

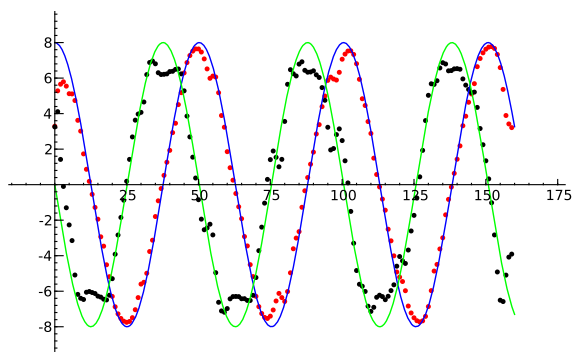


Figure 1.17: Comparison between the estimation of the second order derivate of $x \mapsto \sin(x)$ and the real values, computed with a mask of length 20 and a sample of 400 points.

Discrete Riemann Surfaces

2.1. Conformal maps

Before discretizing conformal maps, it is good to recall what holomorphic and analytic functions are in a visual way, helping to build intuitions and pictures of how the discrete version should behave. This section illustrates this point using a software tool that I have programmed for pedagogical reasons and with which I have produced an article in the CNRS *Images des mathématiques* [3].

Everybody is used to visualizing a function from the plane to the real numbers, like precipitation maps (see Fig. 2.1): simply color the target space \mathbf{R} with colors and plot each point (x, y) of the domain space \mathbf{R}^2 by the color $f(x, y)$. Exactly

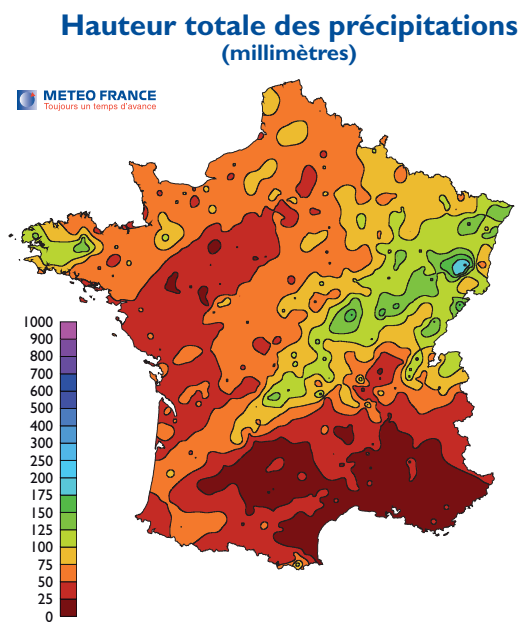


Figure 2.1: Precipitation map in France for July 2009. The color indicates a real value according to the scale. © Météo France

the same can be done with complex valued functions: choose a picture to cover the complex plane seen as the target space, and visualize the function $f : \mathbf{C} \rightarrow \mathbf{C}$ by coloring the point $z \in \mathbf{C}$ with the color $f(z)$.

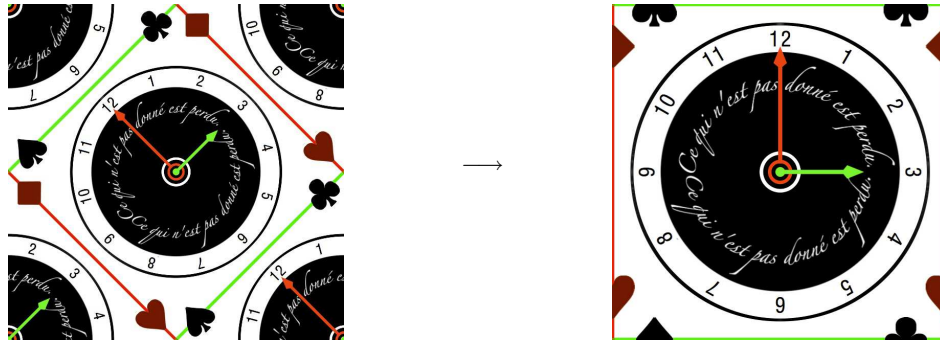


Figure 2.2: The similitude $z \mapsto (1 + i)z$ pictured as the pull-back of the picture of a clock paving the complex plane.

The complex differentiability is visualized by the fact that the picture in the domain space, away from singularities, is to the first order around z , a simple similitude of parameter $1/f'(z)$ since locally, the function behaves as $f(z + z_0) = f(z_0) + z \times f'(z_0) + o(|z|)$. In particular, the zeros of the derivative are very easy to spot since the similitude ratio tends to infinity. There, the function is no longer conformal, it behaves locally as a monomial, $f(z + z_0) - f(z_0) = \frac{f^{(k)}(z_0)}{k!} z^k + o(z^k)$ and the angles through z_0 are divided by k , replicating the features k times.

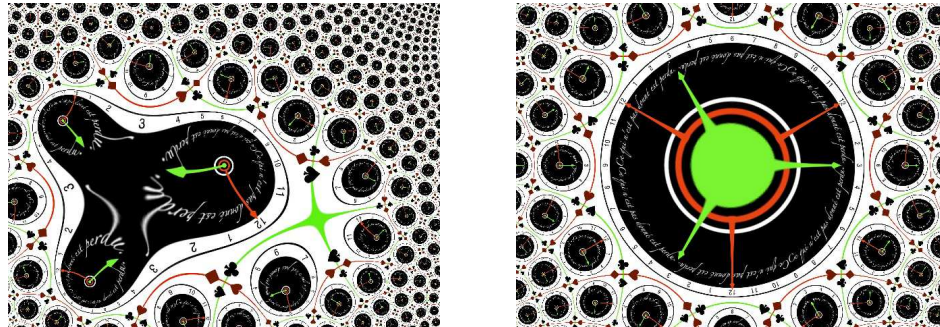


Figure 2.3: The graph of a polynomial and of the monomial $z \mapsto z^3$.

The forward image of a picture by a holomorphic function is much more difficult to obtain, because such a function is not injective, it has a definite degree k and every non critical value in \mathbf{C} is attained exactly k times (see Fig. 2.4).

Although I do have a notion for polynomials in the integrable case, I don't have a good discrete notion for its zeros. The issue is that a zero of high order is difficult to place inside a polygon: since $z \mapsto z^k$ folds k times the plane onto itself, the polygon must have many vertices so that its polygonal image winds k times around the origin. Since we are mainly concerned with quadrilaterals, it is only possible to wind once, zero or minus once around a point, allowing for only one degree of zero and pole, with the extra possibility of degeneracy. Higher degree zeros are seen as

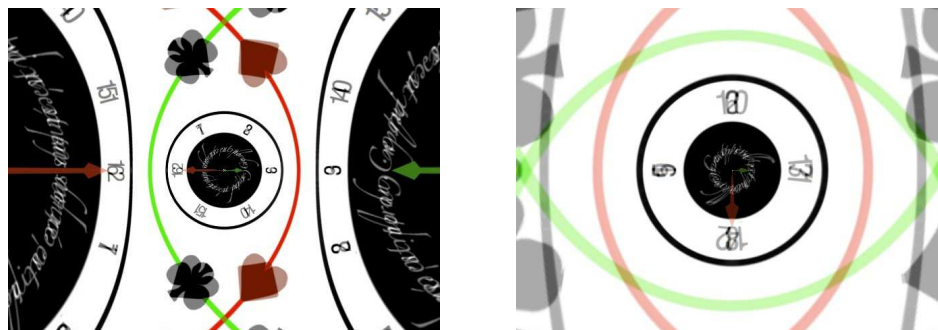


Figure 2.4: The direct images by the square $z \mapsto z^2$ and the cube $z \mapsto z^3$ are blurry, every point is the image of two, resp. three points. They are the pull-back of the multi-valued functions square and cubic roots.

clusters of simple zeros. Another option would be to supplement the values of a function at vertices by integer valued tags.

The integrability of the parallelogram case allows for the expansion of discrete holomorphic functions in series of whether discrete exponentials or discrete polynomials [11].

Together with a student from India, Lalit SIRSIKAR from the Institute of Technology, Banaras Hindu University, we programmed a java applet* based on my previous work with the Java Tools for Experimental Mathematics library† developed by the Technical University Berlin team in which I belonged. This applet lets the user write an expression for a holomorphic function $f(z)$, shows a picture in the target space, as a single tile in a window, its pull-back deformed picture in the domain space in another window. In this domain space, two draggable points, a red and a blue, drive two complex numbers, z_0 and z_1 . Their images $f(z_0), f(z_1)$ by the function f are plotted in the target space, as two points, mapped back to the fundamental tile. A *web-cam* version is as well available, where the picture of the people standing in front of the computer is continuously deformed. I use this applet during special public events and it is very successful with students.

These two points are linked by a polygonal line corresponding to the sequence of TAYLOR *polynomials* of f at z_0 ,

$$S_n(z_1) = f(z_0) + (z_1 - z_0)f'(z_0) + \dots + \frac{(z_1 - z_0)^n}{n!}f^{(n)}(z_0)$$

expressed as a function of z_1 . When the TAYLOR series converges, this polygonal line spirals towards $f(z_1)$, when it diverges, the polygonal lines exhibit different interesting behaviors. A third window shows the pull-back by the last computed TAYLOR polynomial and the disk of convergence of the series is in general very apparent visually as a zone resembling the domain space. This can be probed by moving the blue point in the domain space and witnessing whether the series seems to numerically converge or not, the last bluish point of the polygonal line corresponding to the value of the partial sum in Fig. 2.6. The *inversion* $z \mapsto 1/z$

*<http://www.math.univ-montp2.fr/SPIP/IMG/jar/ComplexImage.jar>

†Java Tools for Experimental Mathematics: <http://jtem.de>

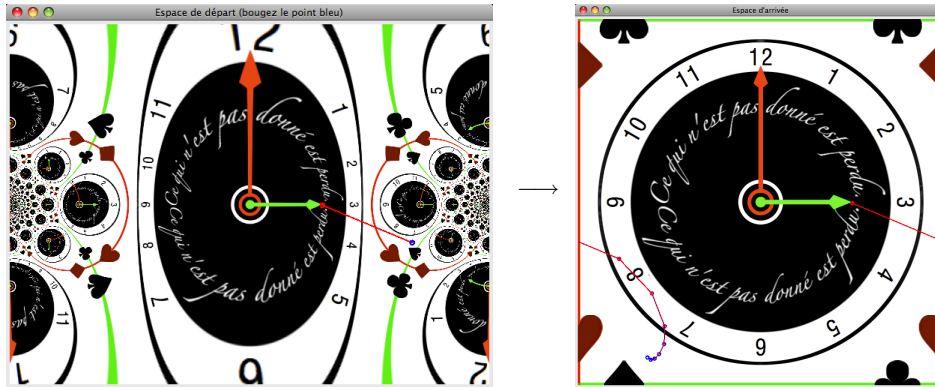


Figure 2.5: The graph of the tangent function $z \mapsto \tan(z)$, on the left, the red point z_0 and the blue point z_1 in the domain space, with the converging polygonal view of the partial TAYLOR sums, from $f(z_0)$ to $f(z_1)$, mapped back to the fundamental tile in the target space.

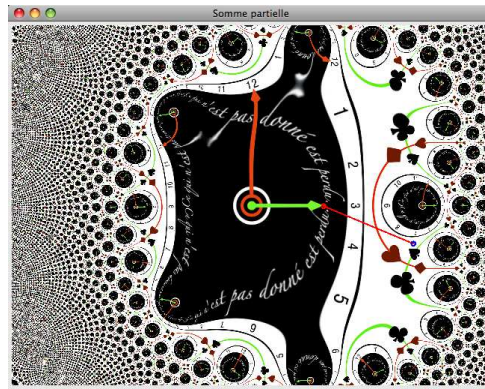


Figure 2.6: The graph of the 8th TAYLOR polynomial of the tangent function $z \mapsto \tan(z)$, expanded at the red point z_0 . The disk of convergence of the series is already discernible as the zone where the difference with Fig. 2.5 is visually not significant.

preserves globally the unit circle, sending inside out, especially exchanging the origin and the infinity. It is a MÖBIUS transformation, sending circles to circles, except circles through the origin which are exchanged with lines (such as the red and green axis lines), see Fig. 2.7. Higher order *poles* $z \mapsto 1/z^k$ are no longer MÖBIUS transformations.

Together with polynomials, they form the field of *rational fractions*. I don't have a good notion for localized poles and their discrete counterparts don't form a canonical field, neither for the multiplication, nor for the composition, without making arbitrary choices.

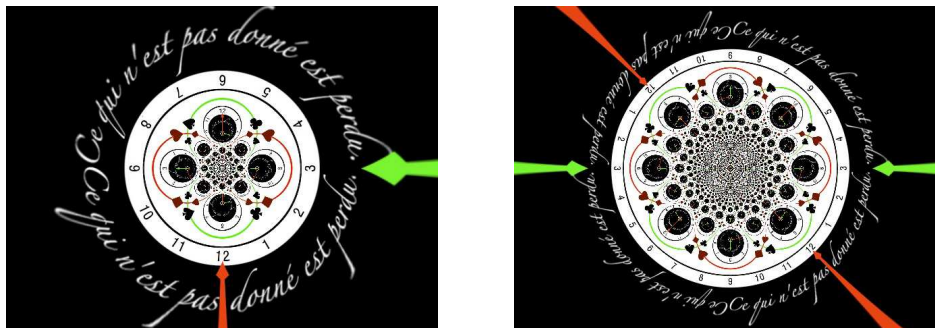


Figure 2.7: The inversion $z \mapsto 1/z$ and a higher degree pole $z \mapsto 1/z^2$.

The *exponential* function is unwrapping centered circles and their rays to vertical and horizontal lines because $x + i\theta \mapsto r \exp(i\theta)$ where $r = \exp(x)$ is the radius of the circle, image of the vertical line at real part x . The exponential is $2i\pi$ -periodic. Its reciprocal, the *logarithm*, is not even a function because it is multi-valued. Given a determination, one has to adjust the vertical size of the tiles to divide $2i\pi$ so that the discontinuity of the tiling synchronizes with the jumps in the determination, giving the illusion of a continuous function, which wraps the horizontal and vertical lines to centered circles and their rays (see Fig. 2.8), showing a logarithmic singularity at the origin. Both notions can be discretized, leading to *discrete exponentials* and the *discrete GREEN function*.

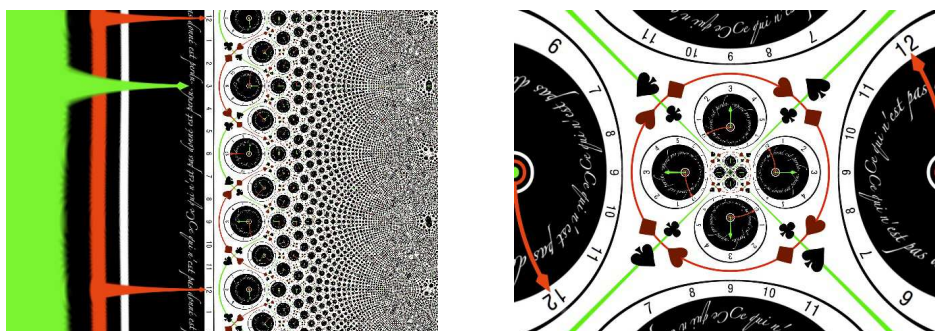


Figure 2.8: The exponential and the logarithm.

The resulting image is invariant under some rotations because the target space is a lattice whose vertical period divides $2i\pi$. But the horizontal period λ of the lattice translates to the invariance by homothety. One can take as a basis of the lattice not $(\lambda, 2i\pi)$ but $(\lambda + 2ik\pi, 2i\pi)$, linking rotation and homothety, obtaining nice *spirals* like in Fig. 2.9.

Beyond zeros of the derivative, poles and logarithmic singularities, an *essential singularity* is an accumulation point of zeros or poles, like in Fig. 2.10.

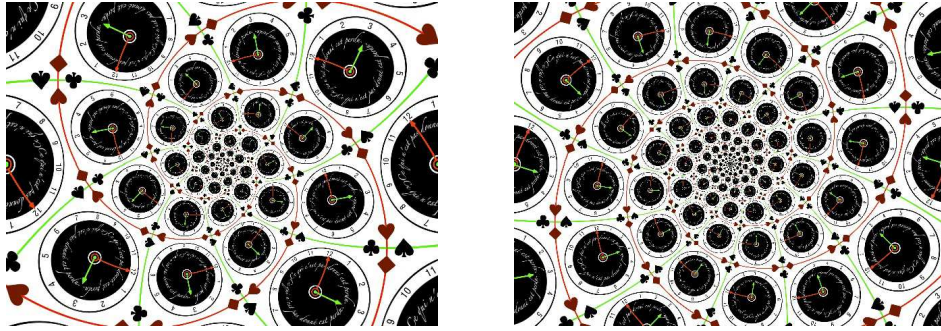


Figure 2.9: The complex logarithm $z \mapsto \log(z) \times (1 + \mu i)$ for appropriate $\mu \in \mathbf{R}$.

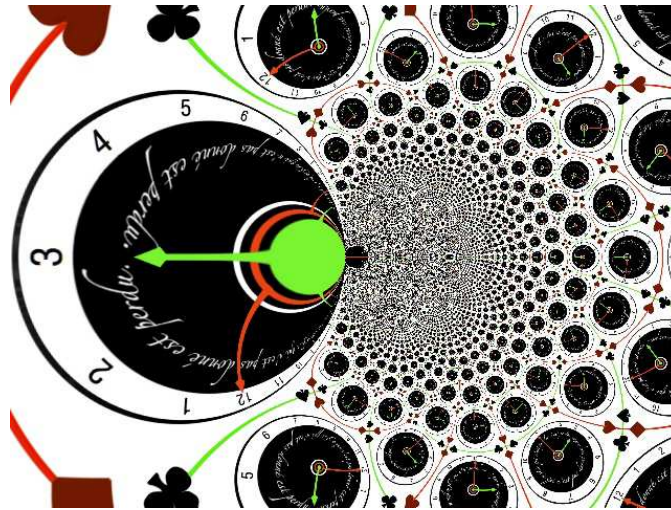


Figure 2.10: The essential singularity of the function $z \mapsto \exp(1/z)$ at the origin, with accumulations of zeros on the negative real side and accumulation of poles on the positive real side.

2.2. Real discrete conformal structure

We begin our discussion of Discrete Complex Analysis by the case when quadrilateral dual diagonals are orthogonal, what I call a *real discrete conformal structure*.

2.2.1. Graphs and Discrete Conformal Structure. Let \diamond a cellular decomposition of an oriented surface by quadrilaterals, that is to say a set \diamond_0 of vertices, linked by a set \diamond_1 of edges, themselves belonging to four-sided faces \diamond_2 . Every edge is attached at most twice to faces. An edge attached only once is a *boundary* edge, twice is an *interior* edge. If the boundary is empty, the surface is *closed*.

We suppose that every loop is of even length (it is the case for trivial loops). Therefore the graph is bipartite and it defines two dual locally planar graphs Γ

and Γ^* , by their vertices $\diamond_0 = \Gamma_0 \sqcup \Gamma_0^*$, their edges $(x, x') \in \Gamma_1$ and $(y, y') \in \Gamma_1^*$, diagonals of the quadrilaterals $(x, y, x', y') \in \diamond_2$. In the closed case, this forms faces $\Gamma_2 \simeq \Gamma_0^*$, $\Gamma_2^* \simeq \Gamma_0$. The boundary case can be handled similarly.

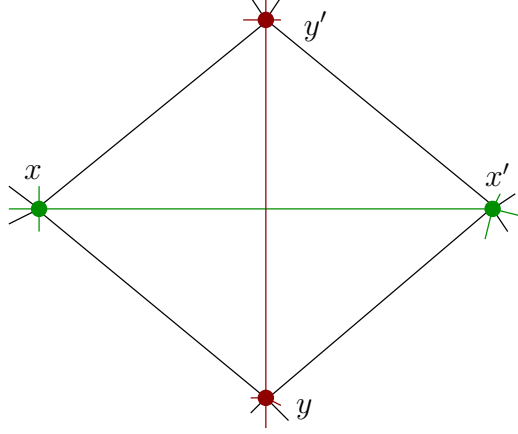


Figure 2.11: Dual edges $(x, x') \in \Gamma_1$ and $(y, y') \in \Gamma_1^*$ are diagonals of a quadrilateral $(x, y, x', y') \in \diamond_2$.

We call the data of a graph Γ , whose unoriented edges are equipped with a positive real number a *discrete conformal structure* and for $e \in \Gamma_1$, we note $\rho(e) > 0$.

We equip the dual graph of positive numbers in the following fashion: In the quadrilateral $(x, y, x', y') \in \diamond_2$, we give to the dual edge $(y, y') = (x, x')^* \in \Gamma_1^*$ the positive real constant $\rho(y, y') = 1/\rho(x, x')$. This number is to be understood later on as the ratio of dual diagonals lengths $\rho(x, x') = \frac{\ell(y, y')}{\ell(x, x')}$.

For commodity, we define $\Lambda := \Gamma \sqcup \Gamma^*$ the *double graph*. The duality exchanges Γ_k and Γ_{2-k}^* , therefore is a bijection in Λ and ρ is defined on Λ_1 such that, for $e \in \Lambda_1$, $\rho(e^*) = 1/\rho(e)$.

2.2.2. Complexes. We recall elements of DE RHAM cohomology: We define the complex of *chains* as the vector spaces spanned by vertices, edges and faces, for each of the above graphs $C(G, \mathbf{R}) = C_0(G, \mathbf{R}) \oplus C_1(G, \mathbf{R}) \oplus C_2(G, \mathbf{R})$. We identify change of orientation of cells and negation of coefficient: for $e \in \Lambda_1$ and $\lambda \in \mathbf{R}$, $\lambda \bar{e} = -\lambda e \in C_1(\Lambda, \mathbf{R})$ is a 1-chain. The 0-chains $C_0(\diamond, \mathbf{R})$ are related to the other 0-chains $C_0(\diamond, \mathbf{R}) \simeq C_0(\Lambda, \mathbf{R})$. For $0 \leq k \leq 2$, $C_k(\Lambda, \mathbf{R}) \simeq C_k(\Gamma, \mathbf{R}) \oplus C_k(\Gamma^*, \mathbf{R})$, with $C_k(\Gamma, \mathbf{R}) \simeq C_{2-k}(\Gamma^*, \mathbf{R})$ through POINCARÉ duality.

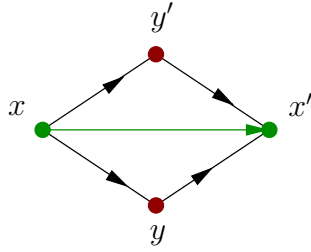
These complexes are equipped with a *boundary operator* $\partial_G : C_k(G) \rightarrow C_{k-1}(G)$, null on vertices, difference of end-points $\partial_G(a, b) = b - a$ on an edge, and sum of the oriented edges forming the boundary of a face. It fulfills $\partial_G^2 = 0$. The kernel $\ker \partial_G =: Z_\bullet(G)$ of the boundary operator are the *closed chains* or *cycles*. Its image are the *exact chains*. It provides the dual spaces of forms, called *cochains*, $C^k(G) := \text{Hom}(C_k(G), \mathbf{R})$ with a *coboundary operator* $d_G : C^k(G) \rightarrow C^{k+1}(G)$ defined by

STOKES formula:

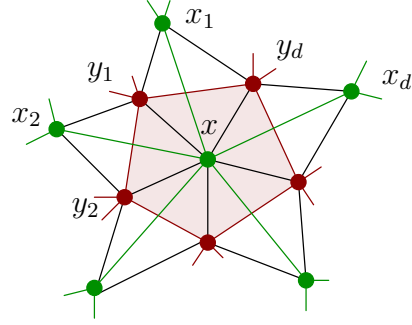
$$\int_{(x,x')} d_G f := f(\partial_G(x,x')) = f(x') - f(x), \quad \iint_F d_G \alpha := \oint_{\partial_G F} \alpha.$$

A *cocycle* is a closed cochain and we note $\alpha \in Z^k(G)$ when $d_G \alpha = 0$.

We will drop the mention of the graph when there is no possible confusion or when the difference is not essential; we can indeed identify closed forms on different graphs under certain conditions:



(2.1)



(2.2)

Figure 2.12: Notations.

2.2.3. Averaging forms. A form on \diamond can be *averaged* into a form on Λ : This map A from $C^\bullet(\diamond)$ to $C^\bullet(\Lambda)$ is the identity for functions of vertices and defined by the following formulae for 1 and 2-forms:

$$(2.1) \quad \int_{(x,x')} A(\alpha_\diamond) := \frac{1}{2} \left(\int_{(x,y)} + \int_{(y,x')} + \int_{(x,y')} + \int_{(y',x')} \right) \alpha_\diamond,$$

$$(2.2) \quad \iint_{x^*} A(\omega_\diamond) := \frac{1}{2} \sum_{k=1}^d \iint_{(x_k, y_k, x, y_{k-1})} \omega_\diamond,$$

where notations are made clear in Fig. 2.12.

The map A is neither injective nor surjective in the non simply-connected case.

Its kernel is $\text{Ker}(A) = \text{Vect}(d_\diamond \varepsilon)$, where ε is the *biconstant*, yielding $+1$ on Γ and -1 on Γ^* .

PROPOSITION 2.2.1. *Averaging carries cocycles on \diamond to cocycles on Λ and its image are the cocycles of Λ verifying that their holonomies along cycles of Λ only depend on their homology on the combinatorial surface*

2.2.4. Hodge star. The HODGE star, in the continuous theory of surfaces is defined on 1-forms, in an orthonormal local coordinates (x, y) , by $*(f dx + g dy) = -g dx + f dy$. In the discrete case the duality transformation plays the role of rotating the orthogonal (x, y) coordinates and the discrete conformal structure takes care of the norm, leading to the following definition:

$$(2.3) \quad \int_{e^*} * \alpha := \rho(e) \int_e \alpha$$

A 1-form $\alpha \in C^1(\Lambda)$ is of *type* $(1, 0)$ if and only if, for each quadrilateral $(x, y, x', y') \in \diamond_2$, $\int_{(y, y')} \alpha = i\rho(x, x') \int_{(x, x')} \alpha$, that is to say if $*\alpha = -i\alpha$. We define similarly forms of type $(0, 1)$ with $+i$ and $-i$ interchanged. A form is *holomorphic*, resp. *anti-holomorphic*, if it is closed and of type $(1, 0)$, resp. of type $(0, 1)$. A function $f : \Lambda_0 \rightarrow \mathbf{C}$ is holomorphic iff $d_\Lambda f$ is. This condition can be rewritten

$$f \text{ is holomorphic} \iff \forall (x, y, x', y) \in \diamond_2, \quad f(y') - f(y) = i\rho(x, x')(f(x') - f(x)).$$

We note $\Omega(\Lambda)$ the space of holomorphic forms.

2.2.5. Wedge product. We construct a wedge product on \diamond such that d_\diamond is a derivation for this product $\wedge : C^k(\diamond) \times C^l(\diamond) \rightarrow C^{k+l}(\diamond)$. It is defined by the following formulae, for $f, g \in C^0(\diamond)$, $\alpha, \beta \in C^1(\diamond)$ and $\omega \in C^2(\diamond)$:

$$\begin{aligned} (f \cdot g)(x) &:= f(x) \cdot g(x) && \text{for } x \in \diamond_0, \\ \int_{(x, y)} f \cdot \alpha &:= \frac{f(x) + f(y)}{2} \int (x, y) \alpha && \text{for } (x, y) \in \diamond_1, \\ \iint_{(x_1, x_2, x_3, x_4)} \alpha \wedge \beta &:= \frac{1}{4} \sum_{k=1}^4 \int_{(x_{k-1}, x_k)} \alpha \int_{(x_k, x_{k+1})} \beta - \int_{(x_{k+1}, x_k)} \alpha \int_{(x_k, x_{k-1})} \beta \\ \iint_{(x_1, x_2, x_3, x_4)} f \cdot \omega &:= \frac{f(x_1) + f(x_2) + f(x_3) + f(x_4)}{4} \iint_{(x_1, x_2, x_3, x_4)} \omega \\ &&& \text{for } (x_1, x_2, x_3, x_4) \in \diamond_2. \end{aligned}$$

The exterior derivative d_\diamond is a derivation for the wedge product, for functions f, g and a 1-form $\alpha \in C^1(\diamond)$:

$$d_\diamond(fg) = f d_\diamond g + g d_\diamond f, \quad d_\diamond(f\alpha) = d_\diamond f \wedge \alpha + f d_\diamond \alpha.$$

We define an *heterogeneous* wedge product for 1-forms living on diagonals Λ_1 , as a 2-form living on faces \diamond_2 . The formula is:

$$(2.4) \quad \iint_{(x, y, x', y')} \alpha \wedge \beta := \frac{1}{2} \left(\int_{(x, x')} \alpha \int_{(y, y')} \beta - \int_{(y, y')} \alpha \int_{(x, x')} \beta \right)$$

Together with the HODGE star, they give rise, in the compact case, to the usual scalar product on 1-forms:

$$(2.5) \quad (\alpha, \beta) := \iint_{\diamond_2} \alpha \wedge * \bar{\beta} = (*\alpha, *\beta) = \overline{(\beta, \alpha)} = \frac{1}{2} \sum_{e \in \Lambda_1} \rho(e) \int_e \alpha \int_e \bar{\beta}$$

The adjoint $d^* = - * d *$ of the coboundary d allows to define the discrete Laplacian $\Delta = d^* d + d d^*$, whose kernel are the harmonic forms and functions. It reads, for a function at a vertex $x \in \Lambda_0$ with neighbours $x' \sim x$:

$$(\Delta f)(x) = \sum_{x' \sim x} \rho(x, x') (f(x) - f(x')).$$

HODGE theorem: The two $\pm i$ -eigenspaces of the star decompose the space of 1-forms, especially the space of harmonic forms, into an orthogonal direct sum.

Types are interchanged by conjugation: $\alpha \in C^{(1,0)}(\Lambda) \iff \bar{\alpha} \in C^{(0,1)}(\Lambda)$ therefore the scalar product decomposes as

$$(\alpha, \beta) = (\pi_{(1,0)}\alpha, \pi_{(1,0)}\beta) + (\pi_{(0,1)}\alpha, \pi_{(0,1)}\beta)$$

where the projections on $(1, 0)$ and $(0, 1)$ spaces are

$$\pi_{(1,0)} = \frac{1}{2}(\text{Id} + i*), \quad \pi_{(0,1)} = \frac{1}{2}(\text{Id} - i*).$$

The harmonic forms of type $(1, 0)$ are the *holomorphic* forms, the harmonic forms of type $(0, 1)$ are the *anti-holomorphic* forms.

2.2.6. Energies. The L^2 norm of the 1-form df , called the DIRICHLET energy of the function f , is the average of the usual DIRICHLET energies on each independant graph

$$(2.6) \quad \begin{aligned} E_D(f) &:= \|df\|^2 = (df, df) = \frac{1}{2} \sum_{(x,x') \in \Lambda_1} \rho(x, x') |f(x') - f(x)|^2 \\ &= \frac{E_D(f|_\Gamma) + E_D(f|_{\Gamma^*})}{2}. \end{aligned}$$

The conformal energy of a map measures its conformality defect, relating these two harmonic functions. A conformal map fulfills the CAUCHY-RIEMANN equation

$$(2.7) \quad * df = -i df.$$

Therefore a quadratic energy whose null functions are the holomorphic ones is

$$(2.8) \quad E_C(f) := \frac{1}{2} \|df - i * df\|^2.$$

It is related to the DIRICHLET energy through the same formula as in the continuous:

$$(2.9) \quad \begin{aligned} E_C(f) &= \frac{1}{2} (df - i * df, df - i * df) \\ &= \frac{1}{2} \|df\|^2 + \frac{1}{2} \|-i * df\|^2 + \text{Re}(df, -i * df) \\ &= \|df\|^2 + \text{Im} \iint_{\diamond_2} df \wedge \bar{df} \\ &= E_D(f) - 2\mathcal{A}(f) \end{aligned}$$

where the area of the image of the application f in the complex plane has the same formula

$$(2.10) \quad \mathcal{A}(f) = \frac{i}{2} \iint_{\diamond_2} df \wedge \bar{df}$$

as in the continuous case. For a face $(x, y, x', y') \in \diamond_2$, the algebraic area of the oriented quadrilateral $(f(x), f(x'), f(y), f(y'))$ is given by

$$\begin{aligned} \iint_{(x,y,x',y')} df \wedge \bar{d}f &= i \operatorname{Im} \left((f(x') - f(x)) \overline{(f(y') - f(y))} \right) \\ &= -2i \mathcal{A}(f(x), f(x'), f(y), f(y')). \end{aligned}$$

2.2.7. Quasi-conformal maps. In the continuous case a function, differentiable as a function of local coordinates (x, y) , can be written, around a point z_0 as

$$f(z + z_0) = f(z_0) + z \times (\partial f)(z_0) + \bar{z} \times (\bar{\partial} f)(z_0) + o(|z|).$$

The complex derivation operators can be defined as small contour integrals:

$$(\partial f)(z_0) = \lim_{\gamma \rightarrow z_0} \frac{i}{2\mathcal{A}(\gamma)} \oint_{\gamma} f d\bar{z}, \quad (\bar{\partial} f)(z_0) = - \lim_{\gamma \rightarrow z_0} \frac{i}{2\mathcal{A}(\gamma)} \oint_{\gamma} f dZ,$$

along a sequence of smaller loops γ around z_0 .

This leads to the discrete definition, when a holomorphic reference map $Z : \Lambda_0 \rightarrow \mathbf{C}$ is chosen, and simply writing u instead of the complex number $Z(u)$,

$$\begin{aligned} \partial : C^0(\diamond) &\rightarrow C^2(\diamond) \\ f &\mapsto \partial f = [(x, y, x', y') \mapsto -\frac{i}{2\mathcal{A}(x, y, x', y')} \oint_{(x, y, x', y')} f d\bar{Z}] \\ &= \frac{(f(x') - f(x))(y' - y) - (\bar{x}' - \bar{x})(f(y') - f(y))}{(x' - x)(y' - y) - (\bar{x}' - \bar{x})(y' - y)}, \end{aligned}$$

$$\begin{aligned} \bar{\partial} : C^0(\diamond) &\rightarrow C^2(\diamond) \\ f &\mapsto \bar{\partial} f = [(x, y, x', y') \mapsto -\frac{i}{2\mathcal{A}(x, y, x', y')} \oint_{(x, y, x', y')} f dZ] \\ &= \frac{(f(x') - f(x))(y' - y) - (x' - x)(f(y') - f(y))}{(x' - x)(y' - y) - (\bar{x}' - \bar{x})(y' - y)}. \end{aligned}$$

A conformal map f fulfills $\bar{\partial} f \equiv 0$ and

$$\partial f(x, y, x', y') = \frac{f(y') - f(y)}{y' - y} = \frac{f(x') - f(x)}{x' - x}.$$

The jacobian $J = |\partial f|^2 - |\bar{\partial} f|^2$ compares the areas:

$$\iint_{(x,y,x',y')} df \wedge \bar{d}f = J \iint_{(x,y,x',y')} dZ \wedge \bar{d}Z.$$

An holomorphic (resp. anti-holomorphic) 1-form df is, locally on each pair of dual diagonals, proportional to dZ , resp. $d\bar{Z}$, so that the decomposition of the exterior derivative into holomorphic and anti-holomorphic parts yields $df \wedge \bar{d}f = (|\partial f|^2 + |\bar{\partial} f|^2) dZ \wedge d\bar{Z}$.

For a discrete function, define the *dilatation* coefficient

$$D_f := \frac{|f_z| + |f_{\bar{z}}|}{|f_z| - |f_{\bar{z}}|}$$

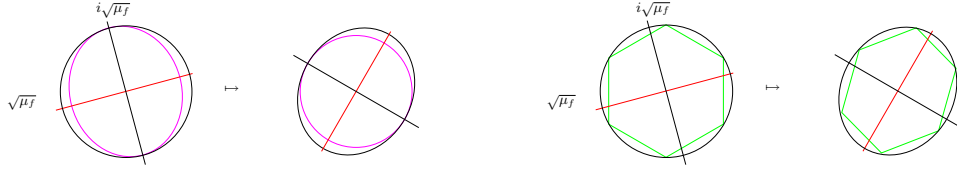


Figure 2.13: Quasi-conformal maps send circles to ellipses, discrete quasi-conformal maps send polygons to non similar polygons (in the spirit of Fig. 3.8, p. 51).

$D_f \geq 1$ for $|f_{\bar{z}}| \leq |f_z|$ (quasi-conformal). Written in terms of the *complex dilatation*:

$$\mu_f = \frac{f_{\bar{z}}}{f_z} = \frac{(f(x') - f(x))(y' - y) - (x' - x)(f(y') - f(y))}{(f(x') - f(x))(\bar{y}' - \bar{y}) - (\bar{x}' - \bar{x})(f(y') - f(y))}.$$

2.2.8. Abelian forms. On a compact surface a basis of the space $\Omega^1(\Lambda)$ of discrete holomorphic 1-forms can be computed [17, 16], in a very similar way as in the continuous, using solutions of (discrete) DIRICHLET and NEUMANN problems for harmonic functions taking values or normal derivative values on some boundary. These problems, in the discrete setup, are finite linear algebra problems with sparse matrices and can be implemented efficiently [8]. They lead to discrete versions of 1-forms with pairs of simple poles and abelian differentials [99, 17].

Despite the similarity, the dimension of $\Omega^1(\Lambda)$ is *twice* the genus of the surface, and one can compute a basis, dual to a normalized homology basis $(a_k, b_k)_{1 \leq k \leq g}$ of the underlying genus g surface:

$$(\zeta_k^\Gamma)_{1 \leq k \leq g} \quad \text{such that} \quad \begin{cases} \oint_{a_k^\Gamma} \zeta_\ell^\Gamma = \delta_{k,\ell}, \\ \oint_{a_k^{\Gamma^*}} \zeta_\ell^\Gamma = 0. \end{cases}$$

and likewise for $(\zeta_k^{\Gamma^*})_{1 \leq k \leq g}$. The 1-form ζ_k^Γ is real on Γ and pure imaginary on Γ^* .

This doubling is characteristic of the discretization process and leads to two period matrices, $\Pi^\Gamma, \Pi^{\Gamma^*}$ on the primal graph Γ and on its dual Γ^* of the holomorphic 1-forms $\zeta_\ell := \zeta_\ell^\Gamma + \zeta_\ell^{\Gamma^*}$:

$$\begin{cases} \Pi_{k,\ell}^\Gamma := \oint_{b_k^\Gamma} \zeta_\ell, \\ \Pi_{k,\ell}^{\Gamma^*} := \oint_{b_k^{\Gamma^*}} \zeta_\ell. \end{cases}$$

These period matrices are equal in the genus one critical case but are otherwise different in general. A challenging issue is that, in that case, a holomorphic 1-form in $\Omega^1(\Lambda)$, which is the bundle of two closed 1-forms on the primal and dual graphs, can not be unified into a closed 1-form on the quad-graph \diamond .

It can be shown and observed numerically [8] (see the following section) that these two period matrices converge to the genuine period matrix of the underlying RIEMANN surface when computed on finer and finer critical discretizations. Numerically wise, it is therefore meaningful to solve the linear system defined by the minimum of the quadratic conformal energy (2.8) for some given monodromy conditions.

Preferring one of these two period matrices and a base point $0 \in \Gamma_0$, allows to define an Abel's map in the Jacobian $\text{Jac}_\Gamma := \mathbf{C}^g / \Lambda_\Gamma$ with Λ_Γ the period lattice

associated with the period matrix Π_Γ :

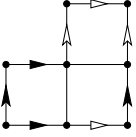
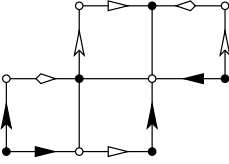
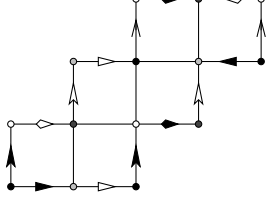
$$\begin{aligned} \Gamma_0 &\longrightarrow \text{Jac}_\Gamma \\ x &\longmapsto \left(\int_0^x \zeta_k\right)_{1 \leq k \leq g} \end{aligned}$$

2.2.9. Numerics with surfaces tiled by squares. In [1], we performed numerical computations of period matrices for flat surfaces with conic singularities and polyhedral surfaces. A number of other methods exist in the literature of geometry processing for discrete conformal parameterization [104, 64, 70, 56, 35, 106, 57, 73, 107], large teams are working on the subject, to cite a few researchers, GU and YAU in Stony-Brook and Harvard, DESBRUN and SCHRÖDER in CalTech, COHEN-STEINER and ALLIEZ in INRIA Sophia-Antipolis, SPRINGBORN, PINKALL, POLTHIER and BOBENKO in Berlin, GOTSMAN and BEN-CHEN at the Technion, and others. In the realm of the ISING model and the dimer model, discrete period matrices using discrete conformal structures have been computed by MC COY and COSTA-SANTOS in [53, 54]

But although their results are visually similar to ours, they are usually not based on a theory of Discrete Complex Analysis as solid and thorough as the present one, with the notable exception of [104], where the link to our theory is still not completely clear. While most geometry processing papers are concerned with efficient algorithms producing beautiful pictures such as [70] and not primarily on the theoretical side of the question, it is quite the contrary in this document, and the following numerics are therefore more a proof of concept and not optimized, the linear algebra library (JTEM) we used is very basic and we stucked to rough double precision.

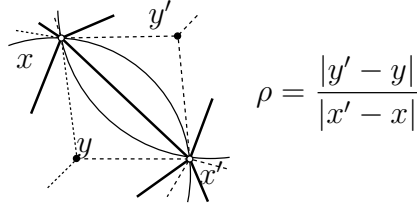
Robert SILHOL supplied us with sets of surfaces tiled by squares for which the period matrices are known [101, 46, 100, 45, 97]. They are translation and half-translation surfaces, each side is identified with a parallel side. The discrete conformal parameter is $\rho \equiv 1$.

The translation surfaces are particularly adapted because the discrete 1-form read off the picture is already a discrete holomorphic form. Therefore the computations are accurate even for a small number of squares and finer squares only blur the result with numerical noise. For half-translation surfaces it is not the case, a continuous limit has to be taken in order to get a better approximation. We computed the approximation of the discrete period matrix using a refinement of the given squares.

Surface & Period Matrix		Numerical Analysis	
 $\Omega_1 = \frac{i}{3} \begin{pmatrix} 5 & -4 \\ -4 & 5 \end{pmatrix}$	#vertices	$\ \Omega_D - \Omega_1\ _\infty$	
	25	$1.13 \cdot 10^{-8}$	
	106	$3.38 \cdot 10^{-8}$	
	430	$4.75 \cdot 10^{-8}$	
	1726	$1.42 \cdot 10^{-7}$	
	6928	$1.35 \cdot 10^{-6}$	
 $\Omega_2 = \frac{1}{3} \begin{pmatrix} -2 + \sqrt{8}i & 1 - \sqrt{2}i \\ 1 - \sqrt{2}i & -2 + \sqrt{8}i \end{pmatrix}$	#vertices	$\ \Omega_D - \Omega_2\ _\infty$	
	14	$3.40 \cdot 10^{-2}$	
	62	$9.51 \cdot 10^{-3}$	
	254	$2.44 \cdot 10^{-3}$	
	1022	$6.12 \cdot 10^{-4}$	
	4096	$1.53 \cdot 10^{-4}$	
 $\Omega_3 = \frac{i}{\sqrt{3}} \begin{pmatrix} 2 & -1 \\ -1 & 2 \end{pmatrix}$	#vertices	$\ \Omega_D - \Omega_3\ _\infty$	
	22	$3.40 \cdot 10^{-3}$	
	94	$9.51 \cdot 10^{-3}$	
	382	$2.44 \cdot 10^{-4}$	
	1534	$6.12 \cdot 10^{-5}$	
	6142	$1.53 \cdot 10^{-6}$	

Using 15 digits numbers, the theoretical numerical accuracy is limited to 8 digits because our energy is quadratic and our error measure $\|\Omega_D - \Omega\|_\infty$ is linear therefore half of the digits are lost. Using an arbitrary precision toolbox or CHOLESKY decomposition in order to solve the linear system would allow for better results but it is not the point here. We see that the convergence is simply of first order. It was shown in [16] that the convergence speed is governed by $1/\sin \theta_{min}$ where θ_{min} is the minimum quad-angle. With squares, this is not an issue.

2.2.10. Polyhedral surfaces. Consider a polyhedral surface in \mathbf{R}^3 . It has a unique DELAUNAY tessellation, generically a triangulation [39]. That is to say each face is associated with a circumcircle drawn on the surface and this disk contains no other vertices than the ones on its boundary. Let's call Γ the graph of this cellular decomposition, Γ_0 its vertices, Γ_1 its edges and complete it into a cellular decomposition with Γ_2 the set of triangles. Each edge $(x, x') = e \in \Gamma_1$ is adjacent to a pair of triangles, associated with two circumcenters y, y' . The ratio of the (intrinsic) distances between the circumcenters and the length of the (orthogonal) edge e defines a discrete conformal structure $\rho(e)$.



For a first test of the numerics on a an immersed surface in \mathbf{R}^3 our choice is the famous CMC-torus discovered by WENTE [108] for which an explicit immersion

formula exists in terms of theta functions [37]. The modulus of the rhombic WENTE torus can be read from the immersion formula:

$$\tau_w \approx 0.41300 \dots + 0.91073 \dots i \approx \exp(i1.145045 \dots).$$

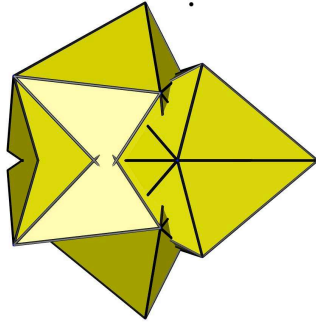
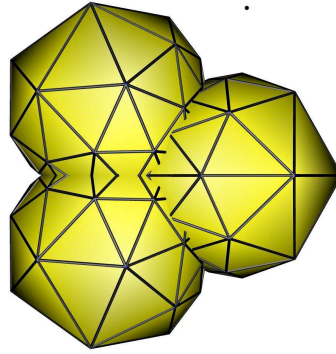
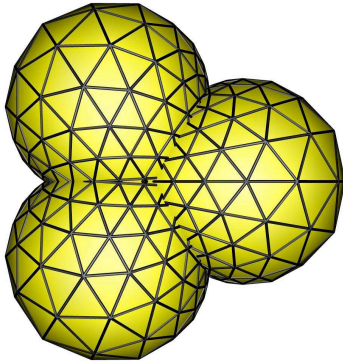
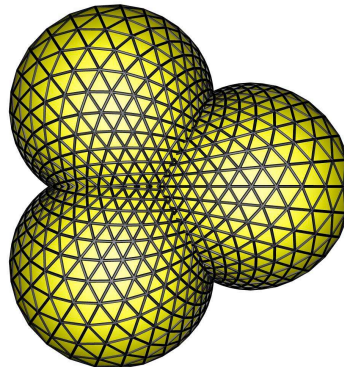
Grid : 10×10 Grid : 20×20 Grid : 40×40 Grid : 80×80

Figure 2.14: Regular DELAUNAY triangulations of the WENTE torus

We compute several regular discretization of the WENTE torus (Fig. 2.14) and generate discrete conformal structure. For a sequence of finer discretizations of a smooth immersion, we compute the modulus which we denote by τ_d and compare them with τ_w from above:

Grid	$\ \tau_d - \tau_w\ $
10×10	$5.69 \cdot 10^{-3}$
20×20	$2.00 \cdot 10^{-3}$
40×40	$5.11 \cdot 10^{-4}$
80×80	$2.41 \cdot 10^{-4}$

Finally we applied our method to compute the period matrix of LAWSON's genus 2 minimal surface in \mathbf{S}^3 [65]. Konrad POLTHIER [92] supplied us with several resolutions. We numerically recognized the period matrix Ω_3 of the third example from Sec. 2.2.9 and verified that the symmetry group of the Lawson genus two surface yields indeed this period matrix, using [27], leading to an algebraic equation for the Lawson surface: $y^2 = x^6 - 1$, with six branch points at the roots of unity. The correspondence between the points in the square picture of the surface and the double sheeted cover of the complex plane is done in Fig. 2.15.

2.2.11. Towards a discrete Riemann-Roch Theorem. In the combinatorial case, BACHER, DE LA HARPE and NAGNIBEDA [28], then BAKER and NORINE in [29] setup the scene and proved a combinatorial RIEMANN-ROCH theorem on graphs. I would like to adapt this very algebraic and combinatorial setup to Discrete Complex Analysis, but I can present here only basic notions and not even a definite conjecture relating them. The issues are that I don't know how to localize a higher degree zero or pole in the discrete case, and that I only know how to define the discrete exponential of the trivial map, $\exp(\lambda z)$ and *not* the exponential of a function $\exp(f(z))$.

We define an *order 1 pole* for a 1-form $\alpha \in C^1(\diamond)$ as a quad-face $Q \in \diamond_2$ where α is of type $(1, 0)$ but is not closed. We call the closeness defect its *residue* at Q : $\text{Res}_Q(\alpha) := \frac{1}{2i\pi} \oint_{\partial Q} \alpha$. Therefore, on a closed discrete manifold \diamond , the sum of all residues of a meromorphic form is null.

We define a *logarithmic singularity* for a function $f \in C^0(\diamond)$ as a quad-face where its exterior derivative df has an order one pole. The function f has locally the features of a GREEN function, its Laplacian is locally non null but 1.

We call $\mathcal{LM}(\diamond)$ the set of meromorphic forms with poles of order 1 and integer residues. It is the formal discrete equivalent of forms $\frac{df}{f}$ with f a meromorphic function on a RIEMANN surface.

Unfortunately, whereas there exists in the critical case a discrete exponential $\exp(\alpha Z)$ for $\alpha \in \mathbf{C}$, there is no discrete equivalent of the exponentiation of an arbitrary meromorphic *function* therefore we can not get a discrete meromorphic function f out of an integer residues 1-form $d \ln f$.

Let's call the free abelian group spanned by quad-faces the *divisor* of the quad-graph: $\text{Div}(\diamond) = \mathbf{Z} \diamond_2$. An element is written as a linear combination of quad-faces, $D = \sum_{Q \in \diamond_2} a_Q Q$, with integer coefficients $D(Q) := a_Q \in \mathbf{Z}$. Its *degree* is their sum, $\text{deg}(D) = \sum_{Q \in \diamond_2} D(Q)$. We note $\text{Div}^k(\diamond)$ the set of divisors of degree k .

Divisors are partially ordered, $D \geq D' \iff \forall Q \in \diamond_2, D(Q) \geq D'(Q)$. A divisor E is called an *effective divisor* if $E \geq 0$. We note $\text{Div}_+(\diamond)$ the set of effective divisors, $\text{Div}_+^k(\diamond)$ the effective divisors of degree k . The *Principal* divisors are the divisors which are in the image of the discrete Laplacian and are of degree zero.

The PICARD group is the quotient of degree zero divisors by principal divisors, $\text{Pic}(G) = \frac{\text{Div}^0(G)}{\text{Prin}(G)}$.

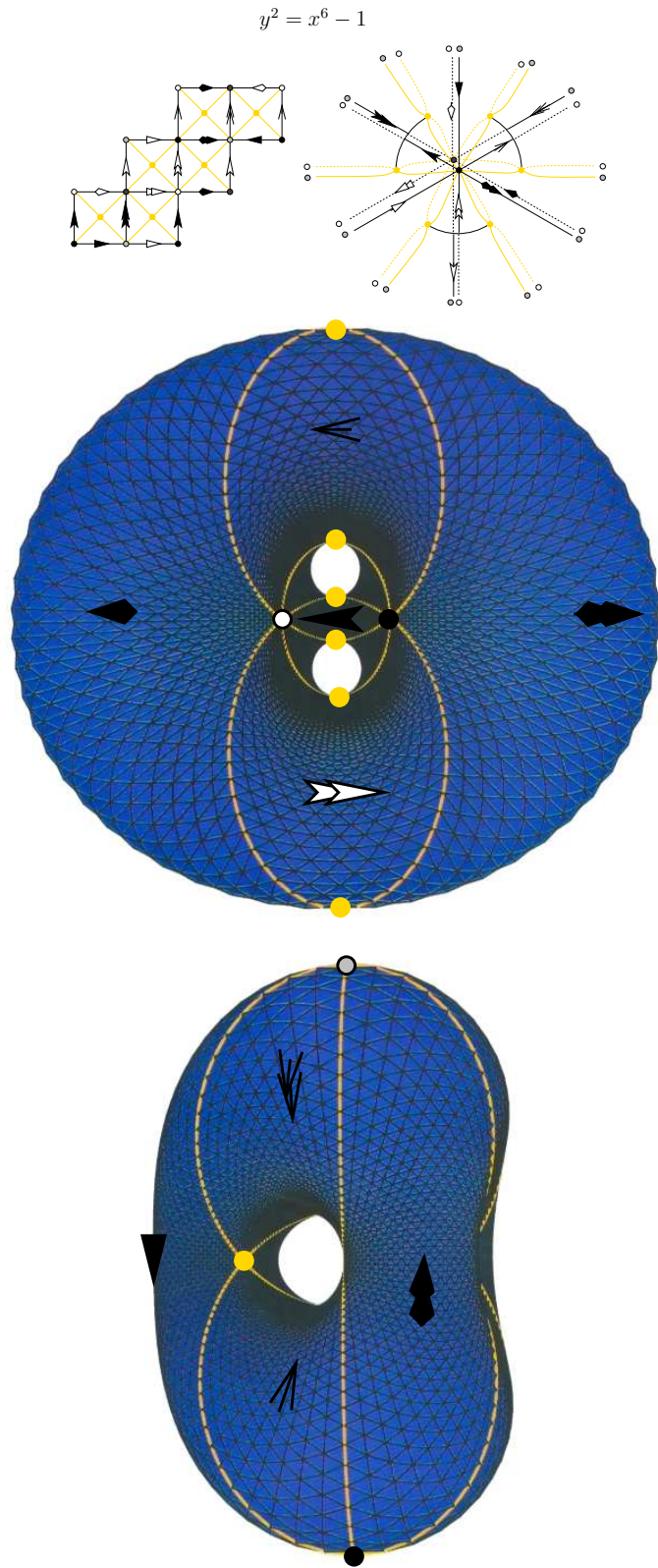


Figure 2.15: The Lawson surface is conformally equivalent to a surface made of squares.

One question that needs to be answered first is, are the PICARD group and the Jacobian, defined by a basis of holomorphic 1-forms, isomorphic? It is related to associating a canonical divisor to a holomorphic 1-form. The degree of this canonical divisor should be related to the genus, $\deg(K) = 2g - 2$.

Does this allow to define an equivalence relations among divisors? Can we compute dimensions of forms associated with certain classes of divisors?

2.3. Non real conformal structure

Triangulations lead to two dual decompositions (Γ, Γ^*) which, taken together, define a quad-graph \diamond . It is true for any cellular decomposition.

There are situations when the cellular decomposition that is available is not a triangulation, when there are some faces which have more than three edges. For example decompositions of a surface by quadrilaterals are more natural in some contexts. A problem then arises, to find the right dual cellular decomposition: there is no canonical circumcenter of four points in 3-space. We will not dwell on this problem and restrict ourselves to the case of quad-meshes, leaving aside the problem of constructing this quad-graph \diamond from a general cellular decomposition, mixing faces of different degrees.

Therefore let's consider as our basic data an oriented quad-graph \diamond in three-space, that is to say a combinatorial data of vertices, edges and commonly oriented faces, $\diamond_0, \diamond_1, \diamond_2$ and an injective map $s : \diamond_0 \rightarrow \mathbf{R}^3$. We require, when the surface is not simply connected, that every closed loop is of even length, so that we can interpret this graph as coming from a couple of dual graphs $\Lambda = \Gamma \oplus \Gamma^*$ whose edges are the diagonals of the quads.

Then we define non real conformal structure constants, for an edge $e \in \Lambda$, $\rho(e) \in \mathbf{C}$.

Each positively oriented quad $(x, y, x', y') \in \diamond_2$ defines two dual edges $(x, x') \in \Gamma$ and $(y, y') \in \Gamma^*$, associated with two vectors $s(x') - s(x), s(y') - s(y) \in \mathbf{R}^3$. Their cross product defines a common *normal* $(s(x') - s(x)) \times (s(y') - s(y))$ along which the four points are projected on the vector space these two vectors span. This plane is identified with the tangent complex plane up to a direct similarity and the two vectors correspond to two complex values $z_{x'x}$ and $z_{y'y}$. The ratio $\rho(x, x') := \frac{z_{y'y}}{iz_{x'x}} \in \mathbf{C}$ defines the complex discrete conformal structure. The normal can be given by other means as well [79].

2.3.1. Complex Hodge star.

DEFINITION 2.3.1. *The HODGE star $*$: $C^1(\Lambda) \rightarrow C^1(\Lambda)$ is defined, on the dual edges $(y, y') = (x, x')^* \in \Lambda_1$, given the (complex) discrete conformal structure $\rho(x, x') = re^{i\theta}$, by*

$$\begin{pmatrix} \int_{(x, x')} * \alpha \\ \int_{(y, y')} * \alpha \end{pmatrix} = \frac{1}{\cos \theta} \begin{pmatrix} -\sin \theta & -\frac{1}{r} \\ r & \sin \theta \end{pmatrix} \begin{pmatrix} \int_{(x, x')} \alpha \\ \int_{(y, y')} \alpha \end{pmatrix}.$$

Notice that the HODGE star is a real transformation and gives back the usual formula (2.3) for real conformal structures.

PROPOSITION 2.3.2. *The HODGE star fulfills $*^2 = -Id_{C^1(\Lambda)}$.*

PROOF 2.3.2. On the quadrilateral $(x, y, x', y') \in \diamond_2$, with the same notations as before,

$$\frac{1}{\cos^2 \theta} \begin{pmatrix} -\sin \theta & -\frac{1}{r} \\ r & \sin \theta \end{pmatrix}^2 = \frac{1}{\cos^2 \theta} \begin{pmatrix} \sin^2 \theta - 1 & 0 \\ 0 & \sin^2 \theta - 1 \end{pmatrix} = -I_2.$$

□

Define its $-i$, respectively $+i$ orthogonal eigenspaces as the type $(1, 0)$, resp. type $(0, 1)$, 1-forms.

With α of type $(1, 0)$, $\int_{(y, y')} \alpha = ir(\cos \theta + i \sin \theta) \int_{(x, x')} \alpha$, which leads to $\int_{(x, x')} * \alpha = -i \int_{(x, x')} \alpha$, likewise along (y, y') , and it is an equivalence. The HODGE star being real, the same result holds for type $(0, 1)$ and $+i$ -eigenspace.

Notice that the scalar product is still positive definite and preserved by $*$ even though the last equality in (2.5) is replaced by a mixed sum over the two dual edges:

$$(2.11) \quad (\alpha, \beta) = \frac{1}{2} \sum_{e \in \Lambda_1} \frac{\int_e \alpha}{\operatorname{Re}(\rho(e))} \left(|\rho(e)|^2 \int_e \bar{\beta} + \operatorname{Im}(\rho(e)) \int_{e^*} \bar{\beta} \right)$$

The DIRICHLET energy mixes the two dual graphs as well:

$$(2.12) \quad E_D(f) := \|df\|^2 = \frac{1}{2} \sum_{e \in \Lambda_1} \frac{|f(x') - f(x)|^2}{\operatorname{Re}(\rho(e))} \left(|\rho(e)|^2 + \operatorname{Im}(\rho(e)) \frac{\overline{f(y') - f(y)}}{f(x') - f(x)} \right).$$

and the Laplacian no longer splits on the two independant dual graphs: For $x_0 \in \Lambda_0$, with dual face $x_0^* = (y_1, y_2, \dots, y_V) \in \Lambda_2$ and neighbours $x_1, x_2, \dots, x_V \in \Lambda_0$, with dual edges $(x_0, x_k)^* = (y_k, y_{k+1}) \in \Lambda_1$, and $y_{V+1} = y_1$,

$$(2.13) \quad \Delta(f)(x_0) = \sum_{k=1}^V \frac{1}{\operatorname{Re}(\rho(e))} (|\rho(e)|^2 (f(x_k) - f(x)) + \operatorname{Im}(\rho(e)) (f(y_{k+1}) - f(y_k)))$$

2.3.2. Surfel surfaces. An important case when the data is given by such quadrilaterals is the case of *surfel surfaces* coming from *voxel* digital objects:

A discrete object is a set of points in \mathbf{Z}^3 , each center of its Voronoi cell is called a *voxel*. A voxel is a cube of unit side, its six faces are called *surfels*. A digital surface Σ made of surfels is a connected set of surfels. We will restrict ourselves to surfaces such that every edge in Σ belongs to at most two surfels [44]. The edges that belong to only one surfel are called *boundary edges*. Let us call (the indices stand for dimensions) $(\diamond_0, \diamond_1, \diamond_2)$ the sets of vertices, edges and surfels of this cellular decomposition \diamond of the surface Σ .

Note that this cellular decomposition is *bipartite*, along the surfels diagonals, their end points form *dual* black and white diagonals and associated Γ and Γ^* cellular decompositions.

The data of a *normal direction* at each surfel is a broadly used feature of digital surfaces [79, 78, 80]. This normal might come from a digital scanner, or be computed from the digital surface itself by various means on which we won't elaborate. These consistent normals give an orientation to the surface.

This normal is used to project a given surfel comprising the four vertices (x, y, x', y') to the *local tangent plane*. This projection deforms the square into

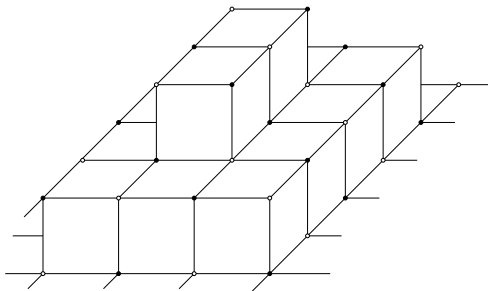
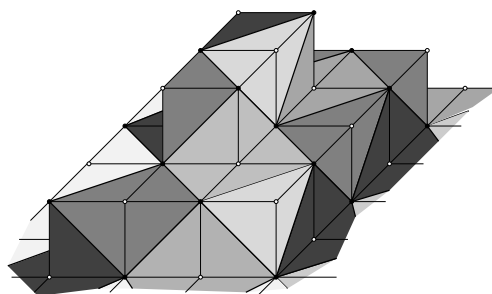


Figure 2.16: A surfel surface

Figure 2.17: The cellular decomposition Γ associated with black vertices

a parallelogram. Its diagonals are sent to segments which are no longer orthogonal in general. We identify the tangent plane with the complex plane, up to the choice of a similitude. We call Z this local map from the cellular decomposition to the complex numbers. Each diagonal (x, x') and (y, y') is now seen as a complex number $Z(x') - Z(x)$, resp. $Z(y') - Z(y)$.

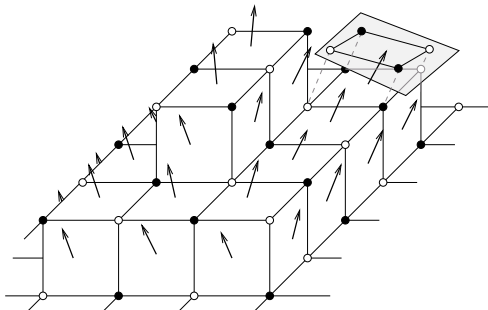


Figure 2.18: A surfel projected onto the local tangent plane

For example we can project the standard digital plane of cubes associated with $P_0 : x + y + z = 0$ onto this (constant tangent) plane P_0 and get the following rhombi pattern.

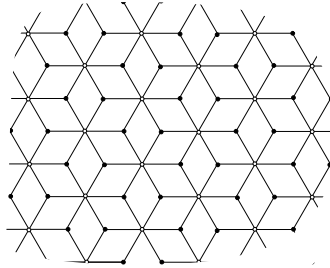


Figure 2.19: The digital plane $x + y + z = 0$ projected. Note that Γ is the hexagonal lattice, Γ^* its triangular dual.

We then associate to each diagonal $(x, x') \in \Gamma_1$ the (possibly infinite) complex ratio $i\rho$ of the dual diagonal by the primal diagonal, as complex numbers.

$$i\rho(x, x') := \frac{Z(y') - Z(y)}{Z(x') - Z(x)}$$

This discrete conformal parameter clearly does not depend on the choice of identification between the tangent plane and the field of complex numbers.

In the standard plane case in Fig. 2.19, its value is the constant $\rho_{\text{hex}} = \tan(\frac{\pi}{6}) = 1/\sqrt{3}$ and its inverse $\rho_{\text{tri}} = \tan(\frac{\pi}{3}) = \sqrt{3} = 1/\rho_{\text{hex}}$. See Fig.1.3 on p. 11 for quad shapes and associated ρ .

An interesting feature of the theory is its robustness with respect to local moves. A discrete holomorphic map defined on a discrete Riemann surface is mapped by a *canonical isomorphism* to the space of discrete holomorphic maps defined on another discrete Riemann surface linked to the original one by a series of *flips*. These flips are called in the context of discrete conformal structures *electrical moves*. They come in three kinds, the third one being the flip, the others being irrelevant to our context.

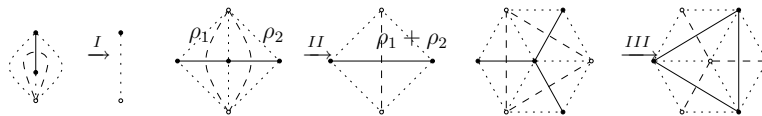


Figure 2.20: The electrical moves.

The third move corresponds to the flip, it is called the *star-triangle transformation*. To three surfels (drawn as dotted lines in Fig. 2.20) arranged in a hexagon,

whose diagonals form a triangle of conformal parameters ρ_1 , ρ_2 and ρ_3 , one associates a configuration of three other surfels whose diagonals form a three branched star with conformal parameters ρ'_i (on the opposite side of ρ_i) verifying

$$(2.14) \quad \rho_i \rho'_i = \rho_1 \rho_2 + \rho_2 \rho_3 + \rho_3 \rho_1 = \frac{\rho'_1 \rho'_2 \rho'_3}{\rho'_1 + \rho'_2 + \rho'_3}.$$

The value of a holomorphic function at the center of an hexagon is overdetermined with respect to the six values on the hexagon. These values have to fulfill a compatibility condition, which are the same for both hexagons, therefore a holomorphic function defined on a discrete Riemann surface can be uniquely extended to another surface differing only by a flip [10].

This means in particular that a discrete holomorphic function defined on the standard plane in Fig. 2.19 can be followed through all its other parallel deformations and is not sensitive to some added noise (flips deleting or inserting extra voxels) provided the normal vector is unchanged with respect to the discrete plane value: the space of holomorphic functions on these parallel or noisy planes are in one-to-one correspondence. This theoretical robustness has yet to be experimentally observed in practice because the normal vectors are not independent and a noisy plane will have noisy normal vectors as well. This will be the subject of a forthcoming article.

Discrete Complex Analysis and Integrability

Consider a *cube*, each face equipped with discrete conformal ratios, whether diagonal ratios ρ or cross-ratios q . The four values, at a corner and at its three neighbors, determine uniquely the three other values of a discrete holomorphic function, by the conditions on each face adjacent to that corner (see Fig. 3.1). But the value at the opposite corner of the cube is then determined by any face among the remaining three. Integrability means a compatibility between the discrete conformal parameters so that the three values coincide.

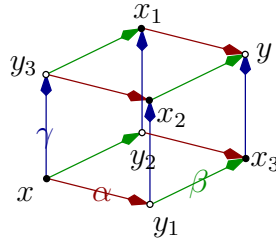


Figure 3.1: The four values $f(x), f(y_1), f(y_2), f(y_3)$ determine uniquely $f(x_1), f(x_2), f(x_3)$ when f is discrete holomorphic, but $f(y)$ is over-determined unless the discrete conformal structure comes from parallelograms.

If we impose that opposite faces in the cube carry the same discrete conformal parameter, then integrability is equivalent to the fact that these parameters come from parallelograms: They are parameterized by quantities constant on *train-tracks* [11, 72]. Two edges opposite in a quadrilateral belong to the same train-track.

The condition of holomorphicity takes place on each quadrilateral, intersection of two train-tracks, labeled by two parameters, as an equation for a function of the four vertices, that the ratio of the values along the diagonals (resp. the cross-ratio), is given by the parameters (see Fig. 3.2).

Integrability means that these equations are compatible, that there exist non trivial solutions (the constant are always solutions).

We showed in [10] that this integrability condition is the same in both the diagonal ratio preserving maps and the cross-ratio preserving maps cases; geometrically it simply means that there exists a discrete holomorphic map made of parallelograms. Moreover, real diagonal ratios ρ and unitary cross-ratios q are associated with rhombi configurations.

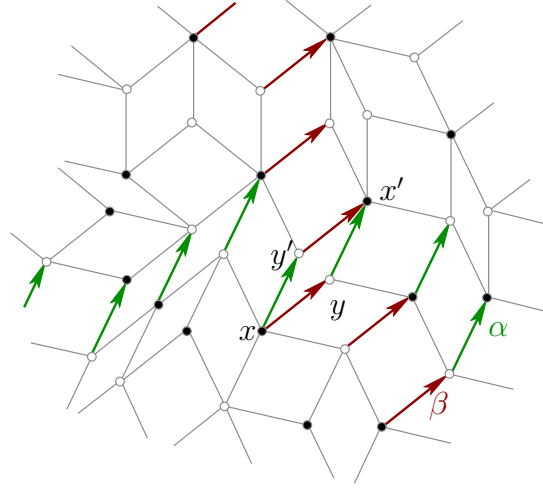


Figure 3.2: Opposite edges in a quadrilateral belong to the same train-track. On the quadrilateral intersection of train-tracks labeled by α and β , consider the equations $\frac{f(y')-f(y)}{f(x')-f(x)} = \frac{\alpha-\beta}{\alpha+\beta}$ for the diagonal ratio preserving maps or $\frac{f(y)-f(x)}{f(x')-f(y)} \frac{f(y')-f(x')}{f(x)-f(y')} = \frac{\beta^2}{\alpha^2}$ for the cross-ratio preserving maps.

3.1. Darboux-Bäcklund transformation

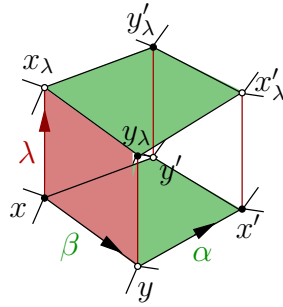
Integrability allows for families of solutions and deformations of existing solutions. Using $3D$ -consistency, one can deform an existing solution, seen as lying at the horizontal *ground floor*, to another floor, at parameter $\lambda \in \mathbf{C}$: Create over each horizontal edge of the quadrilateral, labeled by a certain parameter, a vertical quadrilateral whose vertical edges are labeled by λ , and impose on these vertical faces the same type of equations as for the horizontal faces (see Fig. 3.3).

Diagonal ratio

$$\frac{f(y'_\lambda)-f(y_\lambda)}{f(x'_\lambda)-f(x_\lambda)} = \frac{\alpha-\beta}{\alpha+\beta}$$

$$\frac{f(x_\lambda)-f(y)}{f(y_\lambda)-f(x)} = \frac{\lambda-\beta}{\lambda+\beta}$$

$$\frac{f(y')-f(y)}{f(x')-f(x)} = \frac{\alpha-\beta}{\alpha+\beta}$$



Cross-ratio

$$\frac{f(x_\lambda)-f(y_\lambda)}{f(y_\lambda)-f(x'_\lambda)} \frac{f(x'_\lambda)-f(y'_\lambda)}{f(y'_\lambda)-f(x_\lambda)} = \frac{\beta^2}{\alpha^2}$$

$$\frac{f(x)-f(y)}{f(y)-f(y_\lambda)} \frac{f(y_\lambda)-f(x_\lambda)}{f(x_\lambda)-f(x)} = \frac{\beta^2}{\lambda^2}$$

$$\frac{f(x)-f(y)}{f(y)-f(x')} \frac{f(x')-f(y')}{f(y')-f(x)} = \frac{\beta^2}{\alpha^2}$$

Figure 3.3: DARBOUX-BÄCKLUND transformation: The equations on the vertical quadrilaterals are of the same type as the horizontal ones, whether diagonal ratio or cross-ratio preserving maps.

The function *at the floor* λ fulfills the same equation as the one on the ground floor, that is to say, it is discrete holomorphic. This function, for each parameter

λ , is uniquely defined when an initial value u is chosen at a given point O . This transformation is called the DARBOUX-BÄCKLUND transformation [81]

$$\begin{aligned} B_{\bullet} : \mathbf{C}^2 \times \Omega_0(\diamond) &\rightarrow \Omega_0(\diamond) \\ (\lambda, u, f) &\mapsto B_{\lambda}^u(f) : x \mapsto f(x_{\lambda}) \end{aligned}$$

Let us note $B_{\lambda}^{\rho, u}$, respectively $B_{\lambda}^{q, u}$ the two transformations in the realm of the linear diagonal ration, resp. quadratic cross-ratio preserving maps.

3.2. Zero-curvature representation and isomonodromic solutions

It follows from a result of KENYON and SCHLENKER [72] that any surface made of parallelograms with at most d different train-track parameters, such that no two train-tracks intersect more than once and no train-track with the same parameter self-intersect, can be embedded in such a \mathbf{Z}^d .

The DARBOUX-BÄCKLUND transformation allows to define the holomorphicity condition on a much more general set than cellular decomposition by rhombi. Given d complex numbers $(\alpha_i)_{1 \leq i \leq d}$, define a function f on \mathbf{Z}^d to be discrete holomorphic if, on each quadrilateral parallel to the (i, j) directions, the diagonal ratio, respectively the cross-ratio, of its four values are given by α_i and α_j .

Figure 3.4: On each quadrilateral in \mathbf{Z}^d , impose the linear (a) or quadratic (b) condition.

Solving for one value in terms of the other three values, the conditions (a) and (b) in Fig. 3.4 can be seen as the action of a (non autonomous) operator sitting on directed edges, *a priori* depending on the values on the two other vertices, mapping a third value to the third:

$$(3.1) \quad f(x_{ij}) = L_{ij}(f(x_i), f(x)) \cdot f(x_j)$$

where $L_{ij}(a, b) \in \mathbf{PGL}_2(\mathbf{C})$ acts as a Möbius transformation on \mathbf{C} . The integrability condition is first that this operator is actually defined on the oriented edge $L_{(x, x_i)}$ and does not depend on a face (x, x_i, x_{ij}, x_j) , and second that the discrete connection is *flat*, meaning that the composition of these operators along any closed loop is the identity,

$$(3.2) \quad L_{(x, x_i)} \circ L_{(x_i, x)} = \text{Id}_{\mathbf{PGL}_2(\mathbf{C})}$$

$$(3.3) \quad L_{(x, x_i)} \circ L_{(x_i, x_{ij})} \circ L_{(x_{ij}, x_j)} \circ L_{(x_j, x)} = \text{Id}_{\mathbf{PGL}_2(\mathbf{C})}$$

We give in [10] an explicit zero-curvature representation for both the diagonal ratio and cross-ratio preserving maps which lifts from $\mathbf{PGL}_2(\mathbf{C})$ to a one spectral parameter family of non projective transformations $L_{(x, x_i)} \in \mathbf{GL}_2(\mathbf{C})[\lambda]$:

$$(3.4) \quad \text{Linear case: } L_{(x,x_i)}^p(\lambda) = \begin{pmatrix} \lambda + \alpha_i & -2\alpha_i(f(x) + f(x_i)) \\ 0 & \lambda - \alpha_i \end{pmatrix}$$

$$(3.5) \quad \text{Quadratic case: } L_{(x,x_i)}^q(\lambda) = \begin{pmatrix} 1 & f(x) - f(x_i) \\ \lambda\alpha_i^2/(f(x) - f(x_i)) & 1 \end{pmatrix}$$

We gave the quadratic version as well in terms of the HIROTA variables (see (1.1) on p. 12).

This discrete connection can be composed from the origin into the *moving frame* $\Psi(\lambda; \cdot) : \mathbf{Z}^d \rightarrow GL_2(\mathbf{C})[\lambda]$ defined by prescribing some $\Psi(\lambda; 0)$, and extending it recurrently

$$(3.6) \quad \Psi(\lambda; x_i) = L_{(x,x_i)}(\lambda)\Psi(\lambda; x).$$

The logarithmic derivative of this moving frame with respect to λ

$$(3.7) \quad A(\lambda; x) = \frac{\partial \Psi(\lambda; x)}{\partial \lambda} \Psi^{-1}(\lambda; x)$$

is, for each point $x \in \mathbf{Z}^d$, a meromorphic matrix with respect to λ . Its possible poles are given by the choice of $\Psi(\lambda; 0)$ (or we can choose $A(\lambda; 0)$) as well as $\{\pm\alpha_i\}_{1 \leq i \leq d}$ in the linear case and $\{\pm 1/\sqrt{\alpha_i}\}_{1 \leq i \leq d}$ in the quadratic case.

The definition (3.7) can be rephrased $\frac{\partial \Psi(\lambda; x)}{\partial \lambda} = A(\lambda; x)\Psi(\lambda; x)$, the matrix A governs the dynamic of the moving frame in the spectral parameter direction.

A discrete holomorphic function $f : \mathbf{Z}^d \rightarrow \mathbf{C}$ is called *isomonodromic*, if, for some choice of $A(\lambda; 0)$, the positions and orders of the poles of the matrices $A(\lambda; x)$ do not depend on $x \in \mathbf{Z}^d$.

The GREEN function, the discrete logarithm, is such an isomonodromic solution (see Sec. 3.3.3).

3.3. Integrability and linear theory

What integrability implies is, first of all, the existence of a discrete holomorphic parallelogram immersion of the universal cover of the surface that we will call $Z : \tilde{\diamond}_0 \rightarrow \mathbf{C}$. We will often identify a vertex $z \in \diamond_0$ and its complex image $Z(z)$ to ease the notation.



Figure 3.5: The point z seen as a sum of parallelogram sides from the origin O .

3.3.1. Exponential. It is a rational fraction in the slopes encountered from the origin, for $z = \sum_{k=1}^n \alpha_k$ (see Fig. 3.5):

$$\text{Exp}(\lambda; z) = \prod_{k=1}^n \frac{1 + \frac{\lambda}{2}\alpha_k}{1 - \frac{\lambda}{2}\alpha_k}.$$

It is a generalization of the well known formula where $[Oz]$ is split into n equal segments $\frac{z}{n}$:

$$\exp(\lambda z) = \left(1 + \frac{\lambda z}{n}\right)^n + O\left(\frac{z^2}{n}\right) = \left(\frac{1 + \frac{\lambda z}{2n}}{1 - \frac{\lambda z}{2n}}\right)^n + O\left(\frac{z^3}{n^2}\right).$$

It fulfills the discrete differential equation

$$(3.8) \quad d \operatorname{Exp}(\lambda; z) = \lambda \operatorname{Exp}(\lambda; z) dZ.$$

Derivating it with respect to λ , we define the discrete holomorphic *monomials*

$$(3.9) \quad Z^{:k:}(z) := \left. \frac{\partial^k \operatorname{Exp}(\lambda; z)}{\partial \lambda^k} \right|_{\lambda=0}$$

We have $Z^{:1:} = Z$ and $Z^{:2:} = Z^2$ but discrete values diverge from the point-wise product afterwards. Moreover, apart from the rhombi case (see Sec. 3.3.2), they don't fulfill a nice discrete differential equation such as (3.8).

By TAYLOR's formula, the discrete exponential function is the sum of its TAYLOR series, which is absolutely convergent for $|\lambda| < \frac{2}{\max_i(|\alpha_i|)}$:

$$(3.10) \quad \operatorname{Exp}(\lambda; z) = \sum_{k=0}^{\infty} \frac{\lambda^k Z^{:k:}(z)}{k!}.$$

We proved in [11, 10] that these discrete exponentials (or discrete polynomials) span the space of discrete holomorphic functions (not growing faster than exponentially in the non compact case).

Using KRICHEVER construction, DOLIWA, GRINEVICH, NIESZPORSKI and SANTINI [58] generalize the discrete exponentials to more general spectral curves, the parameter can belong to a Riemann surface with marked points $\lambda \in \Sigma$.

This discrete exponential was as well used in the context of discrete integrable models as the planar waves linear solutions which serve as building blocks of non-linear discrete integrable models named soliton solutions in the framework of *direct linearization* introduced by NIJHOFF, QUISPTEL and CAPEL as early as 1983; this technique is still producing new results [83, 84, 23].

The exponential can be understood in terms of DARBOUX-BÄCKLUND transformations, both linear and quadratic:

PROPOSITION 3.3.1.

$$(3.11) \quad \operatorname{Exp}(\lambda; z) = B_{\frac{z}{\lambda}}^{\rho}(0),$$

$$(3.12) \quad \operatorname{Exp}(\lambda; z) = \left. \frac{\partial}{\partial v} B_{-\lambda}^{q,v}(G) \right|_{v=1}$$

In words, the discrete exponential is the linear DARBOUX-BÄCKLUND transformed of the zero function and spans the kernel of the differential of a composition of the cross-ratio preserving DARBOUX-BÄCKLUND, composed back at the origin. The composition of cross-ratio preserving DARBOUX-BÄCKLUND transformations is a group isomorphism at infinitesimal level and not in general, $B_{\lambda}^{q,v} \circ B_{\mu}^{q,w} \neq B_{\lambda+\mu}^{q,v}$ but nevertheless, the composition $B_{-\lambda}^{q,1} \circ B_{\lambda}^{q,w} = B_0^{q,1} = \operatorname{Id}$ on functions valued 1 at the origin like the exponential, allowing for (3.12).

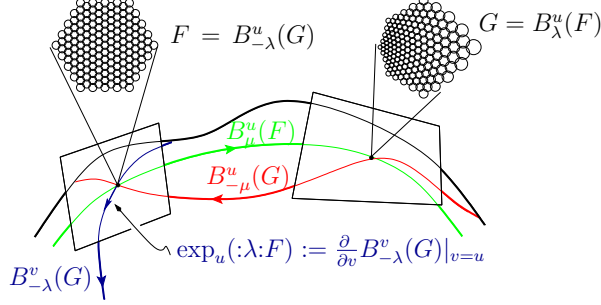


Figure 3.6: The tangent space to the manifold of cross-ratio preserving maps related to an integrable cross-ratio is isomorphic to the space of diagonal ratio preserving maps. The linear discrete exponential is the differential of the cross-ratio preserving DARBOUX-BÄCKLUND transformations composition.

3.3.2. Integration. It was already the case that, for any discrete holomorphic function f and 1-form α , the associated 1-form $f\alpha$ was closed. In the integrable case, when the diagonal ratios are real, that is to say when the parallelograms are all rhombi something special happens:

PROPOSITION 3.3.2. *In the rhombic case, for every discrete holomorphic function f , the 1-form $f dZ$ is as well discrete holomorphic.*

This allows, after the choice of an origin, for the integration of functions on a simply connected quad-graph. Integrating constants, one gets iteratively monomials $Z^{:k:} := k \int_O Z^{:k-1:} dZ$. Notice that the discrete square is equal to the point-wise multiplication $Z^{:2:} = Z^2$, polynomials of degree two are simple restrictions of usual continuous functions, but otherwise, point-wise multiplication doesn't preserve holomorphicity.

The monomials $Z^{:k:}$ provide a basis of discrete holomorphic functions on a compact [11] and more generally among functions not growing faster than exponentially [10]. In particular the discrete exponential is written in terms of polynomials by the usual series (3.10).

Conversely, one can define a *derivation* operator on holomorphic functions. Following Duffin [60], we introduce the

DEFINITION 3.3.3. *For a holomorphic function f , define on a flat simply connected map U the holomorphic functions f^\dagger , the dual of f , and f' , the derivative of f , by the following formulae:*

$$(3.13) \quad f^\dagger(z) := \varepsilon(z) \bar{f}(z),$$

where \bar{f} denotes the complex conjugate, $\varepsilon = \pm 1$ is the biconstant, and

$$(3.14) \quad f'(z) := \frac{4}{\delta^2} \left(\int_O^z f^\dagger dZ \right)^\dagger + \lambda \varepsilon,$$

defined up to ε , with δ the common rhombi side length.

We proved in [16] the following

PROPOSITION 3.3.4. *The derivative f' fulfills*

$$(3.15) \quad df = f' dZ.$$

This derivative allows to give a geometric characterization of discrete holomorphic functions. One has first to visualize an embedding of both dual graphs at the same time by simply *deflating* faces of the graph and of its dual by half. The corresponding vertices meet at the middle of the quad-edges (see Fig. 3.7).

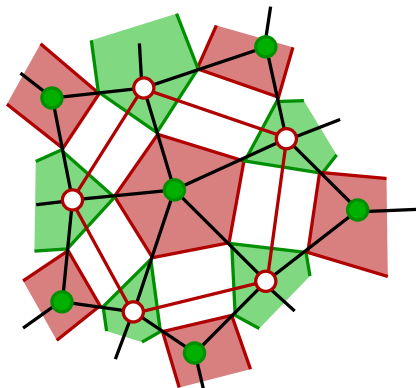


Figure 3.7: Deflating a face by half allows to show both the primal and the dual graphs at the same time.

Then, the closeness condition of $f' dZ$ translates into the fact that the face x^* can be scaled and turned by a factor $f'(x)$, and, when positioned at $f(x)$, still fit together, *kissing* its neighboring faces as in Fig. 3.7, themselves distorted by their respective similarities, given by the derivative ∂f summed up at vertices.

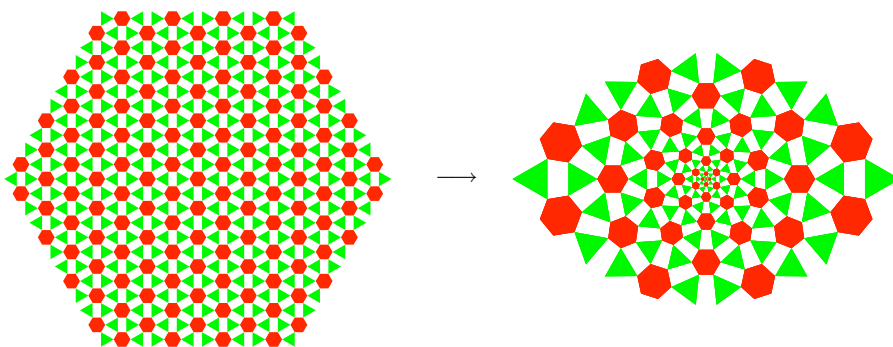


Figure 3.8: The direct image by the cube $z \mapsto z^3$ of the triangular/hexagonal networks as *kissing* equilateral triangles and regular hexagons.

3.3.3. Isomonodromic solutions, the Green function. We now give a construction of a $2d + 1$ dimension family of isomonodromic discrete holomorphic functions in the linear case:

PROPOSITION 3.3.5. *Let there be d sequences $(f_n^{(k)})_{n=0}^\infty$, for $k = 1, \dots, d$, defined by the first two values f_0 and $f_1^{(k)}$ and the recurrent relation*

$$(3.16) \quad n(f_{n+1}^{(k)} - f_{n-1}^{(k)}) = 1 - (-1)^n.$$

Then the discrete holomorphic function $f : (\mathbf{Z}_+)^d \rightarrow \mathbf{C}$, defined by the values $f(n\mathbf{e}_k) = f_n^{(k)}$ on the coordinate semi-axes, is isomonodromic: at any point $z \in (\mathbf{Z}_+)^d$ the associated logarithmic derivative of the moving frame is the following rational fraction, with simple poles at 0 and $\{\pm\alpha_i\}_{1 \leq i \leq d}$,

$$(3.17) \quad A(\lambda; z) = \frac{A^{(0)}(z)}{\lambda} + \sum_{k=1}^d \left(\frac{B^{(k)}(z)}{\lambda + \alpha_k} + \frac{C^{(k)}(z)}{\lambda - \alpha_k} \right),$$

with, for $z = (n_1, \dots, n_d)$,

$$(3.18) \quad A^{(0)}(z) = \begin{pmatrix} 0 & (-1)^{n_1 + \dots + n_d} \\ 0 & 0 \end{pmatrix},$$

$$B^{(k)}(z) = n_k \begin{pmatrix} 1 & -(f(z) + f(z - \mathbf{e}_k)) \\ 0 & 0 \end{pmatrix}, \quad C^{(k)}(z) = n_k \begin{pmatrix} 0 & f(z + \mathbf{e}_k) + f(z) \\ 0 & 1 \end{pmatrix}.$$

which fulfills the following isomonodromic constraint [84], for $z = n_1 \mathbf{e}_1 + \dots + n_d \mathbf{e}_d$,

$$(3.19) \quad \sum_{k=1}^d n_k (f(z + \mathbf{e}_k) - f(z - \mathbf{e}_k)) = 1 - (-1)^{n_1 + \dots + n_d}.$$

Such a solution is *a priori* defined on the positive quadrant but values along the other half axis can be given. The values along the axis are simple:

$$(3.20) \quad \begin{cases} f(2n \mathbf{e}_k) = f_0 \sum_{\ell=1}^n \frac{2}{2\ell-1} & \text{does not depend on } k \text{ and} \\ f((2n+1) \mathbf{e}_k) = f_1^{(k)} & \text{only depends on } k. \end{cases}$$

The discrete GREEN function G is such an isomonodromic solution, associated with the values $f_0 = 0$ and $f_1^{(k)} = \log \alpha_k$. A closed formula for its value at a given point of the positive quadrant $z \in \mathbf{Z}_+^d$ is [71, 10]

$$(3.21) \quad G(z) = \frac{1}{2i\pi} \oint_{\gamma} \frac{\log \lambda}{2\lambda} \text{Exp}(\lambda; z) d\lambda$$

with the proper determination branch for the logarithm and where γ is a loop around the poles $\{\alpha_i\}_{1 \leq i \leq d}$ of the discrete exponential in this positive quadrant. This determination can be followed in other quadrants with other loops around the suitable selection of $\{\pm\alpha_i\}_{1 \leq i \leq d}$. These $2d$ complex numbers are cyclically ordered by their argument, and we patch together $2d$ quadrants associated with this ordering in order to define the subspace in \mathbf{Z}^d where this discrete logarithm is well defined, up to a global $2i\pi$ indeterminacy on odd vertices after each full turn around 0.

Every orientable surface made of parallelograms of slopes α_i can be seen as embedded in this union of quadrants, and any vertex v can be mapped to the origin $0 \in \mathbf{Z}^d$. The restriction of G to this surface provides the inverse of the discrete Laplacian: $\Delta G(x) = \delta_{x,v}$, the (multi-valued) function G is discrete holomorphic hence harmonic, except at the origin v where it has a logarithmic singularity. Of course, proper definitions take place on branched coverings at the origin as for the usual logarithm.

In the rhombic case, the slopes are $\alpha_k = e^{i\theta_k}$, leading to real values on the even sub-graph and pure imaginary values on the odd subgraph. Its restriction to a rhombic surface is likewise split onto real values on the graph Γ , corresponding to $\log |z-v|$ and pure imaginary values on its dual Γ^* (or vice-versa), corresponding to $i \arg(z-v)$. The real part is more often referred to as the discrete Green function.

Isomonodromic solutions for the *quadratic* zero-curvature connection (3.5) can be given [21, 10], in relation to PAINLEVÉ or mKdV equations; they correspond to the cross-ratio preserving and circle pattern versions of $z \mapsto z^\gamma$. It is easy to see that its derivative with respect to γ is the linear isomonodromic GREEN function just described.

Statistical Mechanics

In my thesis, I proved that criticality in the Z-invariant ISING model is characterized by the fact that the fermion ψ becomes a discrete massless DIRAC spinor, that is to say that $\psi \sqrt{dZ}$ is a discrete holomorphic 1-form.

In Australia, with Paul A. PEARCE, at the University of Melbourne, I investigated the *A-D-E* models which generalize the ISING model.

4.1. The critical Ising model

4.1.1. Boltzmann law. The ISING model is defined on a graph Γ , whose edges are labeled by positive ferromagnetic interaction constant $J_{x,x'}$. A state is given by a choice of a spin \pm at each vertex. The probability of a state $\sigma : \Gamma_0 \rightarrow \pm$ is given by the BOLTZMANN weight

$$(4.1) \quad P(\sigma|\sigma_0) = \frac{1}{Z_R} e^{\beta \sum_{(x,x') \in R_1} J_{x,x'} \sigma_x \sigma_{x'}}$$

where R is a finite region, σ_0 is a fixed boundary condition outside R and $Z_R = \sum_{\sigma: R_0 \rightarrow \pm} e^{\beta \sum_{(x,x') \in R_1} J_{x,x'} \sigma_x \sigma_{x'}}$ is the *partition function* such that P is a probability.

It is a model of ferromagnetic spins, they tend to align to their neighbors. The overall parameter $\beta = \frac{1}{k_B T}$ plays the role of the temperature. For low temperature, alignment is much favored (frozen phase), for high temperature, the distribution tends to equiprobability (gas phase). These two regimes can be exchanged by the KRAMERS-WANIER duality [75], exchanging the graph Γ and its dual Γ^* as well as high and low temperatures.

In statistical mechanics, one is interested in taking a *thermodynamic* limit for an infinite graph Γ , when the window R grows to infinity. A phase, or GIBBS measure is a measure on the states such that, when conditioned outside finite regions yields back BOLTZMANN law (4.1) (see [55] in the dimer model).

The free energy per site $f = \lim_{N=|R|} -\frac{\beta}{N} \log Z_R$ is usually analytic in terms of the temperature, except sometimes at special *critical* temperature, witnessing a phase transition between two regimes.

Outside criticality, correlations usually decay exponentially

$$\langle \sigma(x)\sigma(x') \rangle = \sum_{\sigma: \Gamma_0 \rightarrow \pm} P(\sigma) \sigma(x)\sigma(x') \sim |x - x'|^\eta e^{-\frac{|x-x'|}{\xi}}$$

where ξ is the *correlation length*. This correlation length tends to infinity at criticality and leaves a power law decay, $\langle \sigma(x)\sigma(x') \rangle_{T_C} \sim |x - x'|^{-\frac{1}{2}}$ for the ISING model [82]. The critical temperature, in homogeneous situation, is reached at the self-dual temperature for the KRAMERS-WANIER duality (KW). Things are more

complicated in inhomogeneous or aperiodic models [24, 26], correlations satisfy difference equations of the HIROTA type [88].

It was showed by BAXTER [31, 30, 52] that the interaction constant $J_{x,x'}$ could be understood geometrically as coming from a dual/primal length ratio $\rho(x,x') = \text{sh}2\beta J_{x,x'}$ associated with flat rhombi in the critical case. The pair of dual edges compose a quad-graph \diamond .

4.1.2. The fermion ψ . Besides the spin value at a given point, another observable is very interesting, it is the *disorder* operator μ_y , KW-dual of the spin, attached to a path γ in the dual graph Γ_1^* , coming from a fixed point on the boundary, and ending at a given face $y \in \Gamma_0^*$. It consists in flipping the interaction sign along every edge met by the path γ . What is even more fundamental is the correlation of a spin σ_x and the disorder μ_y at an incident face [82]. This observable is

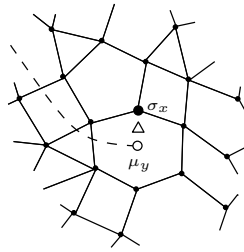


Figure 4.1: The fermion $\psi_{x,y}$ depends on a vertex $x \in \Gamma_0$ and a path γ ending at an incident face $y \in \Gamma_0^*$.

a fermion, they anti-commute and they change sign when one of the two vertices, x or y , makes a full turn around the other. It is actually well-defined on a non trivial double-cover of the discrete direction bundle made of the pairs $\Delta = \{x,y\}$ for $(x,y) \in \diamond_1$.

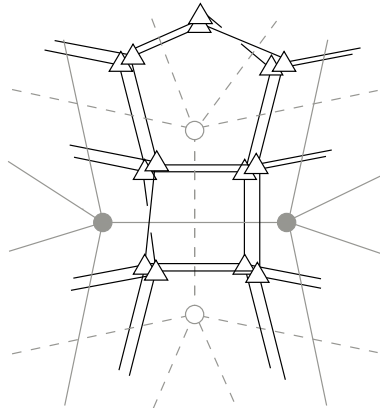


Figure 4.2: Double covering around faces and vertices.

Such fermions can be coupled by pairs and give rise to 1-forms, defined on simply covered oriented edges. Flattening the graph in the plane with a discrete holomorphic function Z provides such a fermion, \sqrt{dZ} .

PROPOSITION 4.1.1. *When the discrete conformal structure is critical, then ψ is a discrete DIRAC spinor:*

$$\psi \sqrt{dZ} \text{ is a discrete holomorphic 1-form.}$$

A continuous limit theorem supports the claim to call such a fermion a discrete massless DIRAC spinor.

The conclusion is that criticality does not need a thermodynamic limit to be identified, it is the point where some statistical mechanics observables become discrete holomorphic.

A massive DIRAC spinor, with elliptic deformations of circular functions can be as well associated with off-criticality.

DIRAC spinors appear as well in the realm of the model of dimers, related to the ISING model and in other situations. Some work has been done recently along these steps, mainly by DE TILIÈRE and BOUTILLIER [41, 42], CIMASONI and RESHETIKHIN [49, 50], CHELKAK and SMIRNOV [103, 48], or PINKALL and BOHLE.

A major achievement was done by SMIRNOV in [102] where he proved the conformal invariance of the critical percolation model, following the steps of LAWLER, SCHRAMM and WERNER [77] but using ideas from discrete holomorphicity.

A great generalization of the DIRAC spinor idea was endeavored by CARDY and RAJABPOUR [93] where they prove that criticality in the \mathbf{Z}_n -parafermion model is implied by the holomorphicity of the 1-form $\psi (dZ)^{\frac{n-1}{n}}$ for ψ the parafermion.

4.2. The critical A - D - E models

The critical A - D - E models correspond, for different choices of regimes and/or fusion level, to unitary minimal models [34], parafermion theories [15] and superconformal theories [96].

4.2.1. A - D - E models. A lattice model in the A - D - E series is associated with a graph of spins G , of A , D or E type. The spins are nodes of the graph G and neighbouring sites on the spatial quad-graph must be neighbouring nodes of the graph. The ISING model corresponds to $A_3 = +-*--$ with a middle frozen state $*$ at the *white* (dual) vertices and two extremal \pm states at the *black* (primal) vertices.

The A - D - E series appear in a variety of contexts. The basic objects are graphs. A simple graph G is given by its *vertices* (or nodes) $a \in G_0$ and *edges* $(a, b) \in G_1 \subset G_0 \times G_0$. We are concerned with unoriented ones, $(a, b) \in G_1 \implies (b, a) \in G_1$. The series is presented in Table 4.3, they are the DYNKIN diagrams of simply laced Lie algebras. The number h is the COXETER number of the graph G and the exponents $Exp(G)$ are a subset (with multiplicities) of the nodes of the A_L graph sharing the same COXETER number as G .

A graph G is completely encoded by its adjacency matrix that we denote by the same letter G . It is a non negative integer square matrix whose rows and columns are labelled by the vertices of G , defined by $G_{ab} = 1$ if and only if a and b are adjacent.

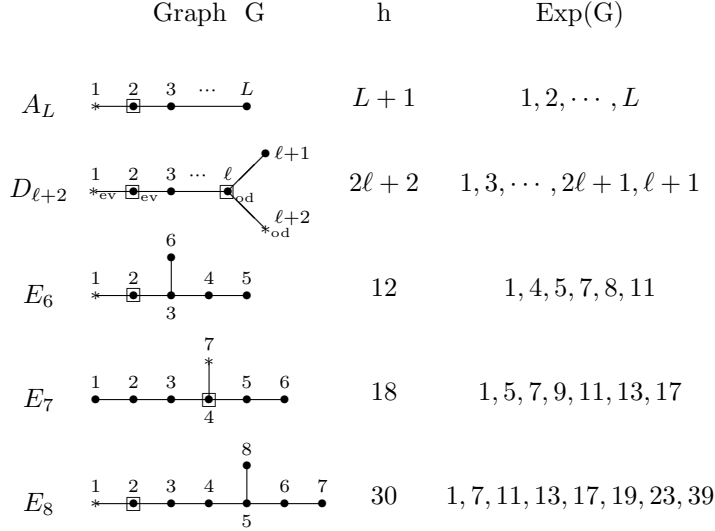


Figure 4.3: DYNKIN diagrams of the classical A - D - E simply laced Lie algebras. The choice of the identity and the fundamental are represented by $*$, \square respectively.

What is so special about these graphs is that (along with the tadpole* series), they are the only one whose spectrum is in the open interval $(-2, 2)$.

The Perron-Frobenius theorem implies that the largest eigenvalue of these transfer matrices is non degenerate, real and positive and its eigenvector can be chosen to have non negative entries. They can be given explicitly in terms of q -deformed integers $S_n = [n]_q = \frac{q^n - q^{-n}}{q - q^{-1}}$ with $q = \exp(i\frac{\pi}{h})$, the largest eigenvalue is $S_2 = [2]_q$ and the eigenvector $\vec{\psi}$ is

$$\begin{aligned}
 \vec{\psi}_{A_L} &= ([k]_q)_{1 \leq k \leq L} \\
 \vec{\psi}_{D_{\ell+2}} &= ([k]_q)_{1 \leq k \leq \ell}, \left[\frac{[\ell]_q}{[2]_q}, \frac{[\ell]_q}{[2]_q} \right] \\
 \vec{\psi}_{E_6} &= ([1]_q, [2]_q, [3]_q, [2]_q, [1]_q, \frac{[3]_q}{[2]_q}) \\
 \vec{\psi}_{E_7} &= ([1]_q, [2]_q, [3]_q, [4]_q, \frac{[6]_q}{[2]_q}, \frac{[4]_q}{[3]_q}, \frac{[4]_q}{[2]_q}) \\
 \vec{\psi}_{E_8} &= ([1]_q, [2]_q, [3]_q, [4]_q, [5]_q, \frac{[7]_q}{[2]_q}, \frac{[5]_q}{[3]_q}, \frac{[5]_q}{[2]_q}).
 \end{aligned}
 \tag{4.2}$$

The DYNKIN diagram $G^{(1)}$ of an affine simply-laced Lie algebra is obtained from the graph G by adding a vertex, linked to the node 2 in the D case, to the short, middle, resp. long leg for E_6 , E_7 , E_8 respectively, and to the first and final nodes in the A case (closing it into a cycle). In these affine cases, the entries of the PERRON-FROBENIUS vector are non negative integers which count the dimensions

*The tadpole graph T_L is obtained from the graph A_L by adding a loop at the final vertex; it is not a simple graph.

of irreducible representations associated with each node. It is one of the reasons why the q -deformed integers associated with the nodes of the graph are referred to as quantum dimensions of quantum analogs of irreducible representations of the quantum-symmetries.

4.2.2. Graph fusion algebra. The integer linear span of the nodes of the graph can be given a structure of a commutative *graph fusion algebra* or PASQUIER algebra [87]. We first specify two vertices, the identity vertex $*$ and the fundamental vertex \square . They are pictured on Table 4.3. They are respectively the vertices labelled 1 and 2 in the A_L , $D_{2\ell+2}$, E_6 and E_8 cases, known as *type I* theories, the vertices $\ell + 1$ and ℓ for the $D_{2\ell+1}$ case, and the vertices 7, 4 (the short leg and the fork node) for the E_7 case, known as *type II* theories

The algebra is defined by stating that the edges of the graph G encode the action of the fundamental element \square :

$$(4.3) \quad a \square = \sum_{b \sim a} b.$$

The identity gives one row of the algebra table, the previous formula gives another, commutativity and associativity determine the rest. On the D_4 example, $\square = 2$ and associativity gives

$$(4.4) \quad \begin{aligned} (4 - 3)(\square \square) &= (4 \square - 3 \square) \square = 0 \\ &= (4 - 3)(1 + 3 + 4) \end{aligned}$$

so that $4 - 3 = 3 \ 3 - 4 \ 4$ and $\square \ 3 \ 3 = \square$ shows that $\begin{cases} 3 \ 3 = 4 \\ 4 \ 4 = 3 \end{cases}$ and the expansion of $3 \ 3 \ 3$ implies $3 \ 4 = 1$.

The structure constants of this algebra are noted \hat{N} :

$$(4.5) \quad ab = \sum_{c \in G} \hat{N}_{ab}^c c.$$

The definition of the algebra implies $\hat{N}_* = I$ and $\hat{N}_\square = G$ and these matrices themselves form an algebra for the usual matrix product:

$$(4.6) \quad \hat{N}_a \cdot \hat{N}_b = \sum_{c \in G} \hat{N}_{ab}^c \hat{N}_c.$$

As it is a commutative algebra containing the adjacency matrix, its common set of eigenvectors is given by the orthogonal basis of eigenvectors of G , they are labelled by COXETER exponents (we have only given the PERRON-FROBENIUS eigenvector ψ^*) and the decomposition of each matrix onto its eigenvectors give these integers through a VERLINDE-like formula:

$$(4.7) \quad \hat{N}_{ab}^c = \sum_{j \in \text{Exp}(G)} \frac{\psi_a^j \psi_b^j (\psi_c^j)^*}{\psi_*^j}.$$

In the case of the graph A_L , it reduces to the usual VERLINDE formula and the structure constants are noted N_{ij}^k and the matrix of eigenvectors, S . Another set of non negative integer matrices algebra with the same structure constants as A_L , is given, for an A - D - E graph G (of type D or E) with the same COXETER number $L + 1$, by the *fused adjacency matrices* n_i defined by the $sl(2)$ recurrence relation

$$(4.8) \quad n_1 = I, \quad n_2 = G, \quad n_{i+1} = n_2 n_i - n_{i-1} \quad \text{for } 2 < i < L,$$

which also verify the VERLINDE like property

$$(4.9) \quad n_{i a}{}^b = \sum_{j \in \text{Exp}(G)} \frac{S_i^j}{S_*^j} \psi_a^j \left(\psi_b^j \right)^*$$

and the algebra structure

$$(4.10) \quad n_i n_j = \sum_{k \in A_L} N_{i j}{}^k n_k.$$

These matrices n_i are in fact linear combinations of the structure constants \hat{N} :

$$(4.11) \quad n_i = \sum_{a \in G} n_{i 1}{}^a \hat{N}_a.$$

For $b \in G$, the rectangular $A_L \times G$ matrix $V^b = (n_{i a}{}^b)_{i \in A_L, a \in G}$ is called an *intertwiner* because it intertwines the fused adjacency matrices:

$$(4.12) \quad N_i V^b = V^b n_i, \quad \forall i \in A_L.$$

Throughout these graph algebras, the idea is that nodes label bimodules and edges are homomorphisms between these bimodules. In the case of the graph G , the edges describe the homomorphisms arising from tensoring with the fundamental bimodule, the result is isomorphic to the direct sum of the bimodules which are adjacent to it on the graph. For type I models, one can associate a graph G_a to each vertex in the same manner, by placing $\hat{N}_{a b}{}^c$ edges between the vertex b and the vertex c . For type II models, this construction fails.

The graph fusion algebra that appears in a PASQUIER A - D - E statistical mechanics models associated with a given graph G is not the graph fusion itself. This latter graph encodes the fusion algebra of a WESS-ZUMINO-WITTEN theory while a PASQUIER A - D - E model is associated with a *minimal model* theory whose fusion algebra is associated with a *double graph* $A_{g-2} \times G$ where g is the COXETER number of G . A vertex of this double graph is of the form $(r, a) \in A_{g-2} \times G$ and is adjacent with the vertex (r', b) whenever whether r and r' , or a and b , are neighbours in A_{g-2} and G respectively. When $G = A_{g-1}$, it is customary to denote such a vertex with the letters (r, s) . The graph fusion algebra for this double graph is simply the tensor product $A_{g-2} \otimes G$ of the two graph fusion algebras. Hence it is generated by the two WZW models subalgebras $1 \otimes G$ and $A_{g-2} \otimes 1$.

4.2.3. Ocneanu algebra. See [51] for a good account on the subject, restricted to WZW models and [91, 90] for a more general point of view. The *Double Triangles Algebra* (DTA), or *Ocneanu algebra* is describing the algebra of boundary conditions [91, 90] or *quantum symmetries* of the problem. It is essentially twice a graph algebra, tensoring a left and a right copies over a subalgebra named the ambichiral algebra. For models of type I, we use the graph algebra itself but it involves the parent theory algebra and a twist for the models of type II. As before, the algebra is determined by a graph, the OCNEANU graph, which has two types of edges (plain and dashed), corresponding to the action of the left and right copies of the generator.

Consider D_4 , the nodes 1, 3, 4 form a \mathbf{Z}_3 subalgebra, the *ambichiral algebra* T . One can then construct the algebra

$$(4.13) \quad D_4 \otimes_{\mathbf{Z}_3} D_4$$

where $a \otimes 3b = a3 \otimes b$ and $a \otimes 4b = a4 \otimes b$ for all $a, b \in D_4$, for example $2 \otimes 3 = 23 \otimes 1 = 2 \otimes 1$. This algebra has six elements, $1 \otimes 1$, $2 \otimes 1$, $1 \otimes 2$, $1 \otimes 3 = 3 \otimes 1$, $1 \otimes 4 = 4 \otimes 1$, $2 \otimes 1 = 2 \otimes 3 = 2 \otimes 4$, $1 \otimes 2 = 3 \otimes 2 = 4 \otimes 2$ and $2 \otimes 2$. It clearly has two generators, a left and a right, $\square_L = 2 \otimes 1$ and $\square_R = 1 \otimes 2$. They generate the *left and right chiral subalgebras*. One would like to encode this algebra in a graph as previously but there is an obstruction:

$$(4.14) \quad (2 \otimes 2)(1 \otimes 2) = 2 \otimes (1 + 3 + 4) = 2 \otimes 1 + 2 \otimes 1 + 2 \otimes 1$$

so while there is only one edge from $2 \otimes 1$ to $2 \otimes 2 = (2 \otimes 1)(1 \otimes 2)$, there would be three in the opposite direction. This problem is solved by splitting the node $2 \otimes 2$ into three different ones, $1', 3', 4'$, using a non central extension of the algebra by an algebra of 2×2 -matrices [51]. The detail of this extension is not needed to compute twisted partition functions. One then obtains the graph presented in Table 2 on p. 62.

The same procedure works for $D_{2\ell}$, it has a $J_{\ell+1}$ sub-algebra generated by the odd vertices (the extremities are both taken as odd) over which the tensor square is taken and extended by an algebra of 2-matrices. In the type I exceptional cases E_6 and E_8 , it is simpler as there is no need to extend the algebra. The subalgebras in these cases are generated by 1, 5, 6 and 1, 7 respectively. The A_L case is yet simpler as we tensorise over the full algebra, yielding the algebra back again: $A_L \otimes_{A_L} A_L \simeq A_L$, all the elements are ambichiral.

In the type II models, $D_{2\ell+1}$ and the exceptional E_7 , the OCNEANU algebra is defined through the twisted square tensor of the parent theory: In the case of $D_{2\ell+1}$, the parent graph is the A -type graph sharing the same Coxeter number, $A_{4\ell-1}$. It has a non trivial automorphism

$$(4.15) \quad \begin{aligned} \rho : A_{4\ell-1} &\rightarrow A_{4\ell-1} \\ a &\mapsto \begin{cases} 4\ell - a & \text{if } a \in \text{Exp } D_{2\ell+1}, \\ a & \text{otherwise.} \end{cases} \end{aligned}$$

The OCNEANU algebra is then defined as $A_{4\ell-1} \otimes_{\rho} A_{4\ell-1}$ where $a \otimes b = a\rho(b) \otimes 1 = 1 \otimes \rho(a)b$. In the E_7 case, the parent theory is D_{10} and the automorphism is given by interchanging the nodes 3 and 10, so that the OCNEANU algebra is $D_{10} \otimes_{T, \rho} D_{10}$ where T is the D_{10} ambichiral subalgebra (its odd vertices, counting forked vertices as both odd).

The OCNEANU algebras just described are the WZW ones. The minimal model OCNEANU algebras are more involved. In particular one can not retrieve in general the WZW OCNEANU algebra as a subalgebra of the minimal model one.

These algebras allow us to write twisted partition functions in conformal field theory with boundary conditions, sesquilinear combinations of extended characters of associated irreducible representations associated to each node (see Table 1).

We identify each of these vertices of the OCNEANU graph, and their incidence relations, to discrete partition functions of exactly solvable A - D - E models, finding their correspondance with integrable and conformal boundary conditions made of fused face operators.

4.2.4. Critical A - D - E models. The A - D - E statistical models are spin models. Each vertex in the spatial quad-graph \diamond is tagged by a spin chosen in the A - D - E graph. Each quadrilateral plaquette is tagged by a spectral parameter u . A state is a spin distribution $\sigma : \diamond_0 \rightarrow G_0$.

$$N_1 = \begin{pmatrix} 1 & 0 & 0 & 0 \\ 0 & 1 & 0 & 0 \\ 0 & 0 & 1 & 0 \\ 0 & 0 & 0 & 1 \end{pmatrix}, \quad N_2 = \begin{pmatrix} 0 & 1 & 0 & 0 \\ 1 & 0 & 1 & 0 \\ 0 & 1 & 0 & 1 \\ 0 & 0 & 1 & 0 \end{pmatrix}, \quad N_3 = \begin{pmatrix} 0 & 0 & 1 & 0 \\ 0 & 1 & 0 & 1 \\ 1 & 0 & 1 & 0 \\ 0 & 1 & 0 & 0 \end{pmatrix}, \quad N_4 = \begin{pmatrix} 0 & 0 & 0 & 1 \\ 0 & 0 & 1 & 0 \\ 0 & 1 & 0 & 0 \\ 1 & 0 & 0 & 0 \end{pmatrix}.$$

	1	2	3	4					
1	1	2	3	4	$Z_1 =$	$\chi_1\chi_1^*$	$+\chi_2\chi_2^*$	$+\chi_3\chi_3^*$	$+\chi_4\chi_4^*$
2	2	1+3	2+4	3	$Z_2 =$	$\chi_2\chi_1^*$	$+(\chi_1+\chi_3)\chi_2^*$	$+(\chi_2+\chi_4)\chi_3^*$	$+\chi_3\chi_4^*$
3	3	2+4	1+3	2	$Z_3 =$	$\chi_3\chi_1^*$	$+(\chi_2+\chi_4)\chi_2^*$	$+(\chi_1+\chi_3)\chi_3^*$	$+\chi_2\chi_4^*$
4	4	3	2	1	$Z_4 =$	$\chi_4\chi_1^*$	$+\chi_3\chi_2^*$	$+\chi_2\chi_3^*$	$+\chi_1\chi_4^*$

$$A_4 \quad \begin{array}{cccc} 1 & 2 & 3 & 4 \\ * & \text{---} & \bullet & \bullet \end{array}$$

Table 1: Fusion matrices, graph fusion algebra and twisted partition functions of A_4 in terms of affine $sl(2)$ characters χ_s .

$$\hat{N}_1 = \begin{pmatrix} 1 & 0 & 0 & 0 \\ 0 & 1 & 0 & 0 \\ 0 & 0 & 1 & 0 \\ 0 & 0 & 0 & 1 \end{pmatrix}, \quad \hat{N}_2 = \begin{pmatrix} 0 & 1 & 0 & 0 \\ 1 & 0 & 1 & 1 \\ 0 & 1 & 0 & 0 \\ 0 & 1 & 0 & 0 \end{pmatrix}, \quad \hat{N}_3 = \begin{pmatrix} 0 & 0 & 1 & 0 \\ 0 & 1 & 0 & 0 \\ 0 & 0 & 0 & 1 \\ 1 & 0 & 0 & 0 \end{pmatrix}, \quad \hat{N}_4 = \begin{pmatrix} 0 & 0 & 0 & 1 \\ 0 & 1 & 0 & 0 \\ 1 & 0 & 0 & 0 \\ 0 & 0 & 1 & 0 \end{pmatrix}.$$

	1	2	3	4					
1	1	2	3	4	$Z_1 =$	$\hat{\chi}_1\hat{\chi}_1^*$	$+\hat{\chi}_3\hat{\chi}_3^*$	$+\hat{\chi}_4\hat{\chi}_4^*$	
2	2	1+3+4	2	2	$Z_{2\otimes 1} =$	$\hat{\chi}_2\hat{\chi}_1^*$	$+\hat{\chi}_2\hat{\chi}_3^*$	$+\hat{\chi}_2\hat{\chi}_4^*$	$= Z_{1\otimes 2}^*$
3	3	2	4	1	$Z_3 =$	$\hat{\chi}_3\hat{\chi}_1^*$	$+\hat{\chi}_4\hat{\chi}_3^*$	$+\hat{\chi}_1\hat{\chi}_4^*$	$= Z_4$
4	4	2	1	3	$Z_4 =$	$\hat{\chi}_4\hat{\chi}_1^*$	$+\hat{\chi}_1\hat{\chi}_3^*$	$+\hat{\chi}_3\hat{\chi}_4^*$	

$$Z_{1'} = Z_{3'} = Z_{4'} = \hat{\chi}_2\hat{\chi}_2^*$$

$$\hat{\chi}_1 = \chi_1 + \chi_5, \quad \hat{\chi}_2 = \chi_2 + \chi_4, \quad \hat{\chi}_3 = \hat{\chi}_4 = \chi_3$$

	1	2	3	4	1'	2'	3'	4'
1	1	2	3	4	1'	2'	3'	4'
2	2	1+3+4	2	2	2'	1'+3'+4'	2'	2'
3	3	2	4	1	3'	2'	4'	1'
4	4	2	1	3	4'	2'	1'	3'
1'	1'	2'	4'	3'	1	2	4	3
2'	2'	1'+3'+4'	2'	2'	2	1+3+4	2	2
3'	3'	2'	1'	4'	3	2	1	4
4'	4'	2'	3'	1'	4	2	3	1

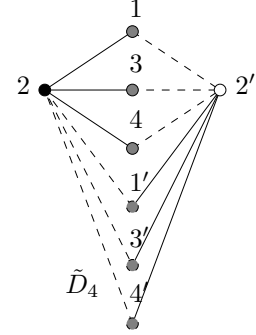


Table 2: Fusion matrices, graph fusion algebra, twisted partition functions, OCNEANU algebra and OCNEANU graph \tilde{D}_4 of D_4 . The extended chiral and ambichiral subalgebras are shown in bold.

The probability distribution of spins is defined by the critical (unfused) BOLTZMANN weight of each plaquette of spins, depending on the spectral parameter u :

$$(4.16) \quad W^{11} \left(\begin{array}{cc|c} d & c & \\ a & b & u \end{array} \right) = \begin{array}{c} d \\ \square \\ a \quad b \end{array} = s(\lambda - u)\delta_{ac} + s(u)\sqrt{\frac{\psi_a\psi_c}{\psi_b\psi_d}}\delta_{bd}$$

where g is the COXETER number of G , $\lambda = \frac{\pi}{g}$, $s(u) = \frac{\sin(u)}{\sin(\lambda)}$ and ψ_a is the entry, associated with the node a , of the PERRON-FROBENIUS eigenvector of the adjacency matrix G .

These BOLTZMANN weights are represented by a local face operator $X_j(u)$ in the TEMPERLEY-LIEB algebra $\mathcal{T}(N, \lambda)$ [34]:

$$(4.17) \quad X_j(u) = \begin{array}{c} \vdots \\ \vdots \\ \text{---} \text{---} \text{---} \\ \text{---} \text{---} \text{---} \\ \vdots \\ \vdots \\ \vdots \end{array} = s(\lambda - u)I + s(u)e_j$$

$\begin{array}{c} \text{---} \text{---} \text{---} \\ \text{---} \text{---} \text{---} \\ \text{---} \text{---} \text{---} \\ \text{---} \text{---} \text{---} \\ \text{---} \text{---} \text{---} \end{array}$

$\begin{array}{c} \text{---} \text{---} \text{---} \\ \text{---} \text{---} \text{---} \\ \text{---} \text{---} \text{---} \\ \text{---} \text{---} \text{---} \\ \text{---} \text{---} \text{---} \end{array}$

where $e_j = X_j(\lambda)$ is a TEMPERLEY-LIEB generator and $j = 1, \dots, N$ labels the position in the lattice.

The algebra is defined by the following identities:

$$(4.18) \quad \begin{aligned} e_j^2 &= s(2\lambda) e_j \\ e_j e_k e_j &= e_j & |j - k| = 1 \\ e_j e_k &= e_k e_j & |j - k| > 1 \end{aligned}$$

4.2.5. Fusion Projector. In turn, this model gives rise to a hierarchy of *fused* models whose Boltzmann weights we are going to describe. They are associated with *blocks* of plaquettes where the internal spins are summed over in a particular way.

We first define recursively the WENZL fusion operators P_j^r , for $r \in \langle 1, g \rangle$ as follows:

$$(4.19) \quad \begin{aligned} P_j^1 &= P_j^2 = I \\ P_j^r &= \frac{1}{S_{r-1}} P_{j+1}^{r-1} X_j(-(r-2)\lambda) P_{j+1}^{r-1}, \quad r \geq 3, \end{aligned}$$

where $S_k = s(k\lambda)$ and j is restricted, resp. periodical in the cylinder, resp. toroidal case [34]. Thus, P_j^r can be expressed as a function of $e_j, e_{j+1}, \dots, e_{j+(r-3)}$. In particular,

$$(4.20) \quad P_j^3 = \frac{1}{S_2} \begin{array}{c} \text{---} \text{---} \text{---} \\ \text{---} \text{---} \text{---} \\ \text{---} \text{---} \text{---} \\ \text{---} \text{---} \text{---} \\ \text{---} \text{---} \text{---} \end{array} = I - \frac{1}{S_2} \begin{array}{c} \text{---} \text{---} \text{---} \\ \text{---} \text{---} \text{---} \\ \text{---} \text{---} \text{---} \\ \text{---} \text{---} \text{---} \\ \text{---} \text{---} \text{---} \end{array}.$$

We shall represent the fusion operators diagrammatically as

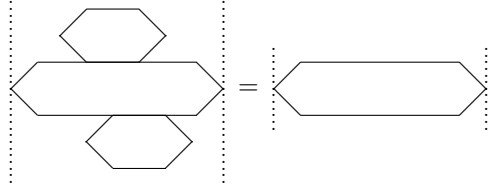
$$(4.21) \quad P_j^r = \begin{array}{c} \vdots \\ \vdots \\ \text{---} \text{---} \text{---} \\ \text{---} \text{---} \text{---} \\ \text{---} \text{---} \text{---} \\ \vdots \\ \vdots \\ \vdots \end{array}$$

$\begin{array}{c} \text{---} \text{---} \text{---} \\ \text{---} \text{---} \text{---} \\ \text{---} \text{---} \text{---} \\ \text{---} \text{---} \text{---} \\ \text{---} \text{---} \text{---} \end{array}$

$\begin{array}{c} \text{---} \text{---} \text{---} \\ \text{---} \text{---} \text{---} \\ \text{---} \text{---} \text{---} \\ \text{---} \text{---} \text{---} \\ \text{---} \text{---} \text{---} \end{array}$

It is easy to show that this operator is in fact a projector. Moreover,

$$(4.22) \quad P_{j'}^{r'} P_j^r = P_j^r P_{j'}^{r'} = P_j^r \quad \text{for } 0 \leq j' - j \leq r - r'.$$



The $+1$ eigenvectors of $P^r(a, b)$ are indexed by an integer $\gamma \in \langle 1, n_r a^b \rangle$ referred to as the *bond variable*. We denote them $\vec{U}_\gamma^r(a, b)$, the *fusion vectors*, also

called *essential paths*. In the A_L case, there is always at most a unique such linear combination of paths while in the D and E cases, the branches allow greater multiplicities, the fused adjacency matrices contains not only 0 and 1 but also some 2. As an example, there are two paths on A_L , going from the node 2 to itself in 2 steps, namely $(2, 1, 2)$ and $(2, 3, 2)$. As they both backtrack, the fusion vector $\vec{U}_1^3(2, 2)$ is unique, proportional to their difference $\psi_3^{\frac{1}{2}}(2, 1, 2) - \psi_1^{\frac{1}{2}}(2, 3, 2)$.

4.2.6. Fused face operators. The fusion projectors allow us to define the (p, q) -fused face operator whose main feature is the product of q rows of p local face operators with a shift of the spectral parameter by $\pm\lambda$ from one face to the next:

$$(4.23) \quad X_j^{pq}(u) = \begin{array}{c} \begin{array}{ccc} & j+p-1 & \\ \vdots & \vdots & \vdots \\ & \text{\textit{X}}^{pq}(u) & \\ \vdots & \vdots & \vdots \\ & j-1 & j+q-1 & j+p+q-2 \end{array} \\ \\ = \begin{array}{c} \begin{array}{ccc} & u+(q-1)\lambda & \\ \vdots & \vdots & \vdots \\ & \text{\textit{X}}^{pq}(u) & \\ \vdots & \vdots & \vdots \\ & P_j^{p+1} & P_{j+q}^{p+1} \\ \vdots & \vdots & \vdots \\ & u-(p-1)\lambda & \end{array} \end{array} \end{array}$$

The position of the projectors and spectral parameters can be altered by *pushing-through*:

$$(4.24) \quad X_j^{pq}(u) = \begin{array}{c} \begin{array}{ccc} & P_{j+p}^{q+1} & \\ \vdots & \vdots & \vdots \\ & u & \\ \vdots & \vdots & \vdots \\ & u-(p-1)\lambda & \\ & P_{j+q}^{p+1} & \end{array} \\ \\ = \begin{array}{c} \begin{array}{ccc} & P_j^{p+1} & P_{j+p}^{q+1} \\ \vdots & \vdots & \vdots \\ & u & \\ \vdots & \vdots & \vdots \\ & u+(q-1)\lambda & \end{array} \\ \\ = \begin{array}{c} \begin{array}{ccc} & P_j^{p+1} & \\ \vdots & \vdots & \vdots \\ & u & \\ \vdots & \vdots & \vdots \\ & P_j^{q+1} & \end{array} \end{array} \end{array}$$

These properties imply several others, namely the *Transposition Symmetry*,

$$(4.25) \quad X_j^{pq}(u)^T = X_j^{qp}(u + (q-p)\lambda),$$

the *Generalized Yang-Baxter Equation (GYBE)*,

$$(4.26) \quad \begin{array}{c} \begin{array}{ccc} & & \\ \vdots & \vdots & \vdots \\ & \text{\textit{X}}^{qp}(v) & \\ \vdots & \vdots & \vdots \\ & \text{\textit{X}}^{qq'}(u+v) & \\ \vdots & \vdots & \vdots \\ & \text{\textit{X}}^{pq'}(u) & \\ \vdots & \vdots & \vdots \\ & & \end{array} \\ \\ = \begin{array}{c} \begin{array}{ccc} & & \\ \vdots & \vdots & \vdots \\ & \text{\textit{X}}^{pq'}(u) & \\ \vdots & \vdots & \vdots \\ & \text{\textit{X}}^{qq'}(u+v) & \\ \vdots & \vdots & \vdots \\ & \text{\textit{X}}^{qp}(v) & \\ \vdots & \vdots & \vdots \\ & & \end{array} \end{array}$$

the *Inversion Relation*,

$$X_j^{pq}(u)X_j^{qp}(-u) = \dots \begin{array}{c} \text{---} \\ \diagdown \quad \diagup \\ X_j^{pq}(u) \quad X_j^{qp}(-u) \\ \diagup \quad \diagdown \\ \text{---} \end{array} \dots$$

$$(4.27) \quad = s_1^{pq}(u) s_1^{qp}(-u) P_j^{q+1} P_{j+q}^{p+1},$$

where $s_i^{pq}(u) = \prod_{j=0}^{p-1} \prod_{k=0}^{q-1} s(u + (i-j+k)\lambda)$ (we will also use the notation s_i^q for $p=1$), and the *Abelian Property*,

$$(4.28) \quad X_j^{pq}(u + (p-1)\lambda)X_j^{qp}(v + (q-1)\lambda) = X_j^{pq}(v + (p-1)\lambda)X_j^{qp}(u + (q-1)\lambda).$$

These operators, contracted against the fusion vectors, yield the (p, q) -fused BOLTZMANN weights. It depends not only on the spins at its four corners but also on bond variables on its edges:

$$W^{pq} \left(\begin{array}{ccc|c} d & \gamma & c & \\ \delta & & \beta & u \\ a & \alpha & b & \end{array} \right) = \begin{array}{c} d \quad \gamma \quad c \\ \delta \quad u \quad \beta \\ a \quad \alpha \quad b \end{array} = \frac{1}{s_0^{pq-1}(u)} \begin{array}{c} d \quad \bar{U}_\gamma^{p-1}(d,c)^\dagger \quad c \\ \bar{U}_\delta^{q-1}(a,b) \quad X^{pq}(u) \quad \bar{U}_\beta^{q-1}(a,b)^\dagger \\ a \quad \bar{U}_\alpha^{p-1}(a,b) \quad b \end{array}$$

$$(4.29)$$

where the function $s_0^{pq-1}(u)$ eliminates some scalar factors common to all the spin configurations which appear in the process of fusion. In the A_L case, we saw that the bond variables are trivial.

These fused BOLTZMANN weights satisfy the following symmetry

$$(4.30) \quad W^{pq} \left(\begin{array}{ccc|c} d & \gamma & c & \\ \delta & & \beta & u \\ a & \alpha & b & \end{array} \right) = \frac{s_0^{qp-1}(u)}{s_0^{pq-1}(u)} W^{qp} \left(\begin{array}{ccc|c} d & \delta & a & \\ \gamma & & \alpha & u + (q-p)\lambda \\ c & \beta & b & \end{array} \right),$$

and *Crossing Symmetry*:

$$(4.31) \quad W^{pq} \left(\begin{array}{ccc|c} d & \gamma & c & \\ \delta & & \beta & u \\ a & \alpha & b & \end{array} \right) = \sqrt{\frac{\psi_a \psi_c}{\psi_b \psi_d}} \frac{s_0^{qp-1}(\lambda-u)}{s_0^{pq-1}(u)} W^{qp} \left(\begin{array}{ccc|c} a & \delta & d & \\ \alpha & & \gamma & \lambda-u \\ b & \beta & c & \end{array} \right).$$

These fused operators, when inserted along a seam, disturb the partition function and we identified one by one the twisted partition functions: We diagonalized large but finite size transfer matrices with inserted seams, renormalized the finite size corrections and recovered the correct list of eigenvalues, associated with characters. The computation of the spectrum for one seam typically took several hours, ending up in *months* of computer number crunching. See Fig. 4.4 for a typical renormalization procedure. This way, we observed numerically the fusion algebra of the continuous theory.

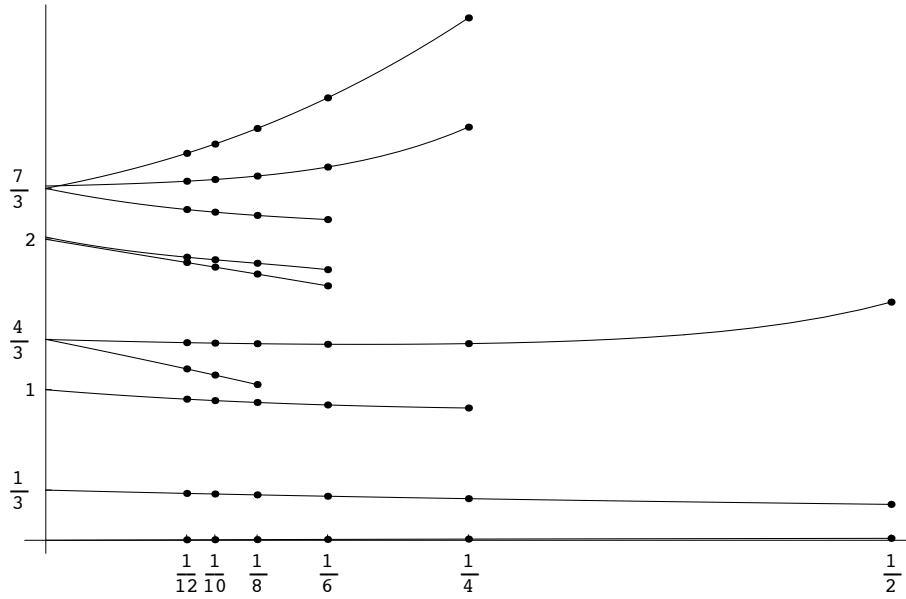


Figure 4.4: Example of extrapolated sequences corresponding to the first ten energy levels of the double row transfer matrix for the A_5 parafermion model with $(1, 3|1, 3)$ boundary conditions, for different number of faces N ; the horizontal axis is $1/N$, the thermodynamic limit corresponds to the vertical axis. The correct character $Z_{13|13}(q) = q^{-1/24}(1 + q^{1/3} + q + 2q^{4/3} + 2q^2 + 3q^{7/3} + 5q^3 + o(q^3))$ and its degeneracy are recovered.

Bibliography

- [1] **B** Alexander Bobenko, Christian Mercat, and Markus Schmies. Conformal structures and period matrices of polyhedral surfaces. In A. Bobenko and Ch. Klein, editors, *Riemann Surfaces - Computational Approaches*, pages 1–13. 2009.
- [2] **C** Ulrich Kortenkamp, Christian Dohrmann, Yves Kreis, Carole Dording, Paul Libbrecht, and Christian Mercat. Using the Intergeo Platform for Teaching and Research. The Ninth International Conference on Technology in Mathematics Teaching (ICTMT 9), Metz, France, July 6-9 (2009).
- [3] **V** Applications conformes. *Images des mathématiques*, Mar. 2009. <http://images.math.cnrs.fr/Applications-conformes.html>.
- [4] **C** Ulrich Kortenkamp, Axel M. Blessing, Christian Dohrmann, Yves Kreis, Paul Libbrecht, and Christian Mercat. Interoperable interactive geometry for europe - first technological and educational results and future challenges of the intergeo project. CERME 6 - Sixth Conference of European Research in Mathematics Education, Lyon, France, Jan. 28-Feb 1 (2009).
- [5] **V** De beaux entrelacs. *Images des mathématiques*, Feb. 2009. <http://images.math.cnrs.fr/De-beaux-entrelacs.html>.
- [6] **C** Discrete complex structure on surfel surfaces. Coeurjolly, David (ed.) et al., Discrete geometry for computer imagery. 14th IAPR international conference, DGCI 2008, Lyon, France, April 16–18, 2008. Proceedings. Berlin: Springer. Lecture Notes in Computer Science 4992, 153-164 (2008)., 2008.
- [7] **C** Paul Libbrecht, Cyrille Desmoulins, Ch. M., Colette Laborde, Michael Dietrich, and Maxim Hendriks. Cross-curriculum search for Intergeo. Autexier, Serge (ed.) et al., Intelligent computer mathematics. 9th international conference, AISC 2008, 15th symposium, Calculemus 2008, 7th international conference, MKM 2008, Birmingham, UK, July 28–August 1, 2008. Proceedings. Berlin: Springer. Lecture Notes in Computer Science 5144. Lecture Notes in Artificial Intelligence, 520-535 (2008)., 2008.
- [8] **B** Discrete riemann surfaces. In Athanase Papadopoulos, editor, *Handbook of Teichmüller Theory, vol. I*, volume 11 of *IRMA Lect. Math. Theor. Phys.*, pages 541–575. Eur. Math. Soc., Zürich, 2007.
- [9] **V** Keltische Flechtwerke. *Spektrum der Wissenschaft*, Special issue Ethnomathematik:46–51, Nov. 2006. <http://www.spektrum.de/artikel/856963>.
- [10] **A** Alexander I. Bobenko, Ch. M., and Yuri B. Suris. Linear and nonlinear theories of discrete analytic functions. Integrable structure and isomonodromic Green’s function. *J. Reine Angew. Math.*, 583:117–161, 2005.
- [11] **A** Exponentials form a basis of discrete holomorphic functions on a compact. *Bull. Soc. Math. France*, 132(2):305–326, 2004.
- [12] **A** C. H. O. Chui, Ch. M., and Paul A. Pearce. Integrable and conformal twisted boundary conditions for $sl(2)$ A - D - E lattice models. *J. Phys. A*, 36(11):2623–2662, 2003.
- [13] **B** C. H. Otto Chui, Ch. M., and Paul A. Pearce. Integrable boundaries and universal TBA functional equations. In *MathPhys odyssey, 2001*, volume 23 of *Prog. Math. Phys.*, pages 391–413. Birkhäuser Boston, Boston, MA, 2002.
- [14] **A** C. H. Otto Chui, Ch. M., William P. Orrick, and Paul A. Pearce. Integrable lattice realizations of conformal twisted boundary conditions. *Phys. Lett. B*, 517(3-4):429–435, 2001.

- [15] A Ch. M. and Paul A. Pearce. Integrable and conformal boundary conditions for Z_k parafermions on a cylinder. *J. Phys. A*, 34(29):5751–5771, 2001.
- [16] A Discrete Riemann surfaces and the Ising model. *Comm. Math. Phys.*, 218(1):177–216, 2001.
- [17] T Holomorphie discrète et modèle d’Ising. PhD thesis, Université Louis Pasteur, Strasbourg, France, 1998. under the direction of Daniel Bennequin, Prépublication de l’IRMA, available at <http://www-irma.u-strasbg.fr/irma/publications/1998/98014.shtml>.
- [18] V Les entrelacs des enluminures celtes. *Pour la Science*, (Numéro Spécial Avril), 1997. www.entrelacs.net.
- [19] V Théorie des nœuds et enluminure celte. *l’Ouvert*, Num. 84:1–22, 1996, IREM de Strasbourg.

- A Peer reviewed article
- B Peer reviewed book chapter
- C Peer reviewed conference proceeding
- T PhD Thesis
- V Non peer reviewed vulgarization

- [20] V.E. Adler, A.I. Bobenko, and Yu.B. Suris. Classification of integrable equations on quad-graphs. The consistency approach. *Commun. Math. Phys.*, 233(3):513–543, 2003.
- [21] Sergey I. Agafonov and Alexander I. Bobenko. Discrete Z^7 and Painlevé equations. *Internat. Math. Res. Notices*, (4):165–193, 2000.
- [22] Marc Alexa, Michael Kazhdan, and Konrad Polthier, editors. Berlin, Germany, 2009. Eurographics Association.
- [23] James Atkinson, Jarmo Hietarinta, and Frank Nijhoff. Soliton solutions for Q3. 2008.
- [24] Helen Au-Yang and Jacques H. H. Perk. Critical correlations in a Z -invariant inhomogeneous Ising model. *Phys. A*, 144(1):44–104, 1987.
- [25] Helen Au-Yang and Jacques H. H. Perk. Correlation functions and susceptibility in the Z -invariant Ising model. In *MathPhys odyssey, 2001*, volume 23 of *Prog. Math. Phys.*, pages 23–48. Birkhäuser Boston, Boston, MA, 2002.
- [26] Helen Au-Yang and Jacques H. H. Perk. Wavevector-dependent susceptibility in aperiodic planar Ising models. In *MathPhys odyssey, 2001*, volume 23 of *Prog. Math. Phys.*, pages 1–21. Birkhäuser Boston, Boston, MA, 2002.
- [27] M. V. Babich, A. I. Bobenko, and V. B. Matveev. Solution of nonlinear equations, integrable by the inverse problem method, in Jacobi theta-functions and the symmetry of algebraic curves. *Izv. Akad. Nauk SSSR Ser. Mat.*, 49(3):511–529, 672, 1985.
- [28] Roland Bacher, Pierre de la Harpe, and Tatiana Nagnibeda. The lattice of integral flows and the lattice of integral cuts on a finite graph. *Bull. Soc. Math. France*, 125(2):167–198, 1997.
- [29] Matthew Baker and Serguei Norine. Riemann-Roch and Abel-Jacobi theory on a finite graph. *Adv. Math.*, 215(2):766–788, 2007.
- [30] R. J. Baxter. Solvable eight-vertex model on an arbitrary planar lattice. *Philos. Trans. Roy. Soc. London Ser. A*, 289(1359):315–346, 1978.
- [31] Rodney J. Baxter. *Exactly solved models in statistical mechanics*. Academic Press Inc. [Harcourt Brace Jovanovich Publishers], London, 1989. Reprint of the 1982 original.
- [32] Vladimir V. Bazhanov, Vladimir V. Mangazeev, and Sergey M. Sergeev. Faddeev-Volkov solution of the Yang-Baxter equation and discrete conformal symmetry. *Nucl. Phys., B*, 784(3):234–258, 2007.
- [33] Arnaud Beauville. Conformal blocks, fusion rules and the Verlinde formula. In *Proceedings of the Hirzebruch 65 Conference on Algebraic Geometry (Ramat Gan, 1993)*, volume 9 of *Israel Math. Conf. Proc.*, pages 75–96, Ramat Gan, 1996. Bar-Ilan Univ.
- [34] Roger E. Behrend and Paul A. Pearce. Integrable and conformal boundary conditions for $\widehat{\mathfrak{sl}}(2)$ A - D - E lattice models and unitary minimal conformal field theories. In *Proceedings*

- of the Baxter Revolution in Mathematical Physics (Canberra, 2000), volume 102, pages 577–640, 2001. [hep-th/0006094](#).
- [35] M. Ben-Chen, C. Gotsman, and G. Bunin. Conformal Flattening by curvature prescription and metric scaling. In *Computer Graphics Forum*, 27(2). Proc. Eurographics, 2008.
- [36] Itai Benjamini and Oded Schramm. Harmonic functions on planar and almost planar graphs and manifolds, via circle packings. *Invent. Math.*, 126(3):565–587, 1996.
- [37] A. I. Bobenko. All constant mean curvature tori in \mathbf{R}^3 , S^3 , H^3 in terms of theta-functions. *Math. Ann.*, 290(2):209–245, 1991.
- [38] Alexander Bobenko and Ulrich Pinkall. Discrete isothermic surfaces. *J. Reine Angew. Math.*, 475:187–208, 1996.
- [39] Alexander I. Bobenko and Boris A. Springborn. A discrete Laplace–Beltrami operator for simplicial surfaces. *Discrete Comput. Geom.*, 38(4):740–756, 2007.
- [40] Alexander I. Bobenko and Yuri B. Suris. Discrete Koenigs nets and discrete isothermic surfaces. *Int. Math. Res. Not. IMRN*, 2009(11):1976–2012, 2009.
- [41] Cédric Boutillière and Béatrice de Tilière. The critical Z -invariant Ising model via dimers: the periodic case. *To appear in Probab. Theory Relat. Fields*, 2008.
- [42] Cédric Boutillière and Béatrice de Tilière. The critical Z -invariant Ising model via dimers: locality property. 2009.
- [43] Ulrike Bücking. Approximation of conformal mappings by circle patterns. *Geom. Dedicata*, 137:163–197, 2008.
- [44] Jasmine Burguet and Rémy Malgouyres. Strong thinning and polyhedral approximation of the surface of a voxel object. *Discrete Appl. Math.*, 125(1):93–114, 2003. 9th International Conference on Discrete Geometry for Computer Imagery (DGCI 2000) (Uppsala).
- [45] Peter Buser and Robert Silhol. Geodesics, periods, and equations of real hyperelliptic curves. *Duke Math. J.*, 108(2):211–250, 2001.
- [46] Peter Buser and Robert Silhol. Some remarks on the uniformizing function in genus 2. *Geom. Dedicata*, 115:121–133, 2005.
- [47] A. Cappelli, C. Itzykson, and J.-B. Zuber. Modular invariant partition functions in two dimensions. *Nuclear Phys. B*, 280(3):445–465, 1987.
- [48] Dmitry Chelkak and Stanislav Smirnov. Discrete complex analysis on isoradial graphs. [math.CV/0810.2188](#), pages 1–31, 2008.
- [49] David Cimasoni and Nicolai Reshetikhin. Dimers on surface graphs and spin structures. I. *Commun. Math. Phys.*, 275(1):187–208, 2007.
- [50] David Cimasoni and Nicolai Reshetikhin. Dimers on surface graphs and spin structures. II. *Commun. Math. Phys.*, 281(2):445–468, 2008.
- [51] Robert Coquereaux and Gil Schieber. Twisted partition functions for adic boundary conformal field theories and oceanu algebras of quantum symmetries. [hep-th/0107001:1–47](#), 2001.
- [52] Ruben Costa-Santos. Geometrical aspects of the Z -invariant Ising model. *Eur. Phys. J. B*, 53(1):85–90, 2006.
- [53] Ruben Costa-Santos and Barry M. McCoy. Dimers and the critical Ising model on lattices of genus > 1 . *Nucl. Phys., B*, 623(3):439–473, 2002.
- [54] Ruben Costa-Santos and Barry M. McCoy. Finite size corrections for the Ising model on higher genus triangular lattices. *J. Stat. Phys.*, 112(5-6):889–920, 2003.
- [55] Béatrice de Tilière. Quadri-tilings of the plane. *Probab. Theory Relat. Fields*, 137(3-4):487–518, 2007.
- [56] M. Desbrun, M. Meyer, and P. Alliez. Intrinsic parameterizations of surface meshes. *Computer Graphics Forum*, (21):209–218, 2002.
- [57] Mathieu Desbrun, Eva Kanso, and Yiyang Tong. Discrete differential forms for computational modeling. In *SIGGRAPH '06: ACM SIGGRAPH 2006 Courses*, pages 39–54, New York, NY, USA, 2006. ACM Press.
- [58] A. Doliwa, P. Grinevich, M. Nieszporski, and P. M. Santini. Integrable lattices and their sublattices: from the discrete Moutard (discrete Cauchy–Riemann) 4-point equation to the self-adjoint 5-point scheme. *J. Math. Phys.*, 48(1):013513, 28, 2007.
- [59] R. J. Duffin. Basic properties of discrete analytic functions. *Duke Math. J.*, 23:335–363, 1956.
- [60] R. J. Duffin. Potential theory on a rhombic lattice. *J. Combinatorial Theory*, 5:258–272, 1968.

- [61] I. A. Dynnikov and S. P. Novikov. Geometry of the triangle equation on two-manifolds. *Mosc. Math. J.*, 3(2):419–438, 742, 2003. Dedicated to Vladimir I. Arnold on the occasion of his 65th birthday.
- [62] Jacqueline Ferrand. Fonctions préharmoniques et fonctions préholomorphes. *Bull. Sci. Math. (2)*, 68:152–180, 1944.
- [63] Katarzyna Gebal, J. Andreas Bærentzen, Henrik Aanæs, and Rasmus Larsen. Shape Analysis Using the Auto Diffusion Function. In Alexa et al. [22], pages 1405–1413.
- [64] Xianfeng Gu and Shing-Tung Yau. Global conformal surface parameterization. In *SGP '03: Proceedings of the 2003 Eurographics/ACM SIGGRAPH symposium on Geometry processing*, pages 127–137, Aire-la-Ville, Switzerland, Switzerland, 2003. Eurographics Association.
- [65] Jr. H.B. Lawson. Complete minimal surfaces in s^3 . *Ann. of Math.*, (92):335–374, 1970.
- [66] Udo Hertrich-Jeromin. Transformations of discrete isothermic nets and discrete cmc-1 surfaces in hyperbolic space. *Manuscripta Math.*, 102(4):465–486, 2000.
- [67] Tim Hoffmann. Discrete cmc surfaces and discrete holomorphic maps. In *Discrete integrable geometry and physics (Vienna, 1996)*, volume 16 of *Oxford Lecture Ser. Math. Appl.*, pages 97–112. Oxford Univ. Press, New York, 1999.
- [68] Tim Hoffmann. Discrete Hashimoto surfaces and a doubly discrete smoke-ring flow. In *Discrete differential geometry*, volume 38 of *Oberwolfach Semin.*, pages 95–115. Birkhäuser, Basel, 2008.
- [69] Tim Hoffmann. On discrete differential geometry and its links to visualization. In *Consortium “Math for Industry” First Forum*, volume 12 of *COE Lect. Note*, pages 45–51. Kyushu Univ. Fac. Math., Fukuoka, 2008.
- [70] Miao Jin, Yalin Wang, Shing-Tung Yau, and Xianfeng Gu. Optimal global conformal surface parameterization. In *VIS '04: Proceedings of the conference on Visualization '04*, pages 267–274, Washington, DC, USA, 2004. IEEE Computer Society.
- [71] Richard Kenyon. The Laplacian and Dirac operators on critical planar graphs. *Invent. Math.*, 150(2):409–439, 2002.
- [72] Richard Kenyon and Jean-Marc Schlenker. Rhombic embeddings of planar quad-graphs. *Trans. Amer. Math. Soc.*, 357(9):3443–3458 (electronic), 2005.
- [73] Liliya Kharevych, Boris Springborn, and Peter Schröder. Discrete conformal mappings via circle patterns. *ACM Trans. Graph.*, 25(2):412–438, 2006.
- [74] Christer Kiselman. Functions on discrete sets holomorphic in the sense of Ferrand, or monodiffric functions of the second kind. *Sci. China Ser. A*, 51(4):604–619, 2008.
- [75] H. A. Kramers and G. H. Wannier. Statistics of the two-dimensional ferromagnet. I. *Phys. Rev. (2)*, 60:252–262, 1941.
- [76] Robert P. Langlands, Marc-André Lewis, and Yvan Saint-Aubin. Universality and conformal invariance for the Ising model in domains with boundary. *J. Statist. Phys.*, 98(1-2):131–244, 2000.
- [77] Gregory F. Lawler, Oded Schramm, and Wendelin Werner. Conformal invariance of planar loop-erased random walks and uniform spanning trees. *Ann. Probab.*, 32(1B):939–995, 2004.
- [78] Alexandre Lenoir. Fast estimation of mean curvature on the surface of a 3d discrete object. In *DGCI '97: Proceedings of the 7th International Workshop on Discrete Geometry for Computer Imagery*, pages 175–186, London, UK, 1997. Springer-Verlag.
- [79] Alexandre Lenoir, Rémy Malgouyres, and Marinette Revenu. Fast computation of the normal vector field of the surface of a 3-D discrete object. In *Discrete geometry for computer imagery (Lyon, 1996)*, volume 1176 of *Lecture Notes in Comput. Sci.*, pages 101–112. Springer, Berlin, 1996.
- [80] Rémy Malgouyres. A discrete radiosity method. In *Discrete geometry for computer imagery (Bordeaux, 2002)*, volume 2301 of *Lecture Notes in Comput. Sci.*, pages 428–438. Springer, Berlin, 2002.
- [81] V. B. Matveev. Darboux transformations, covariance theorems and integrable systems. In *L. D. Faddeev’s Seminar on Mathematical Physics*, volume 201 of *Amer. Math. Soc. Transl. Ser. 2*, pages 179–209. Amer. Math. Soc., Providence, RI, 2000.
- [82] Barry M. McCoy, Jacques H. H. Perk, and Tai Tsun Wu. Ising field theory: quadratic difference equations for the n -point Green’s functions on the lattice. *Phys. Rev. Lett.*, 46(12):757–760, 1981.
- [83] F. W. Nijhoff, G. R. W. Quispel, and H. W. Capel. Direct linearization of nonlinear difference-difference equations. *Phys. Lett. A*, 97(4):125–128, 1983.

- [84] F. W. Nijhoff, A. Ramani, B. Grammaticos, and Y. Ohta. On discrete Painlevé equations associated with the lattice KdV systems and the Painlevé VI equation. *Stud. Appl. Math.*, 106(3):261–314, 2001.
- [85] Adrian Ocneanu. Paths on Coxeter Diagrams: From Platonic Solids and Singularities to Minimal Models and Subfactors. *Lectures on Operator Theory, Fields Institute, AMS*, 1995.
- [86] Vincent Pasquier. Exact solubility of the D_n series. *J. Phys. A*, 20(4):L217–L220, 1987.
- [87] Vincent Pasquier. Two-dimensional critical systems labelled by Dynkin diagrams. *Nuclear Phys. B*, 285(1):162–172, 1987.
- [88] J. H. H. Perk. Quadratic identities for Ising model correlations. *Phys. Lett. A*, 79(1):3–5, 1980.
- [89] V. B. Petkova and J.-B. Zuber. Generalised twisted partition functions. *Phys. Lett. B*, 504(1-2):157–164, 2001.
- [90] V. B. Petkova and J.-B. Zuber. The many faces of Ocneanu cells. *Nuclear Phys. B*, 603(3):449–496, 2001.
- [91] Valentina Petkova and Jean-Bernard Zuber. Conformal field theories, graphs and quantum algebras. In *MathPhys odyssey, 2001*, volume 23 of *Prog. Math. Phys.*, pages 415–435. Birkhäuser Boston, Boston, MA, 2002.
- [92] Ulrich Pinkall and Konrad Polthier. Computing discrete minimal surfaces and their conjugates. *Experiment. Math.*, 2(1):15–36, 1993.
- [93] M. A. Rajabpour and J. Cardy. Discretely holomorphic parafermions in lattice Z_N models. *J. Phys. A*, 40(49):14703–14713, 2007.
- [94] J.-P. Reveillès. *Géométrie discrète, Calcul en nombres entiers et algorithmique*. PhD thesis, Université Louis Pasteur, Strasbourg, France, 1991.
- [95] J.R. Reyes Martínez. Correlation functions for the Z -invariant Ising model. *Phys. Lett., A*, 227(3-4):203–208, 1997.
- [96] Christoph Richard and Paul A. Pearce. Integrable lattice realizations of $N = 1$ superconformal boundary conditions. *Nucl. Phys., B*, 631(3):447–470, 2002.
- [97] Rubí E. Rodríguez and Víctor González-Aguilera. Fermat’s quartic curve, Klein’s curve and the tetrahedron. In *Extremal Riemann surfaces (San Francisco, CA, 1995)*, volume 201 of *Contemp. Math.*, pages 43–62. Amer. Math. Soc., Providence, RI, 1997.
- [98] Oded Schramm. Circle patterns with the combinatorics of the square grid. *Duke Math. J.*, 86(2):347–389, 1997.
- [99] C. L. Siegel. *Topics in complex function theory. Vol. II*. Wiley Classics Library. John Wiley & Sons Inc., New York, 1988. Automorphic functions and abelian integrals, Translated from the German by A. Shenitzer and M. Tretkoff, With a preface by Wilhelm Magnus, Reprint of the 1971 edition, A Wiley-Interscience Publication.
- [100] R. Silhol. Period matrices and the Schottky problem. In *Topics on Riemann surfaces and Fuchsian groups (Madrid, 1998)*, volume 287 of *London Math. Soc. Lecture Note Ser.*, pages 155–163. Cambridge Univ. Press, Cambridge, 2001.
- [101] Robert Silhol. Genus 2 translation surfaces with an order 4 automorphism. In *The geometry of Riemann surfaces and abelian varieties*, volume 397 of *Contemp. Math.*, pages 207–213. Amer. Math. Soc., Providence, RI, 2006.
- [102] Stanislav Smirnov. Critical percolation and conformal invariance. In *XIVth International Congress on Mathematical Physics*, pages 99–112. World Sci. Publ., Hackensack, NJ, 2005.
- [103] Stanislav Smirnov. Towards conformal invariance of 2D lattice models. In *International Congress of Mathematicians. Vol. II*, pages 1421–1451. Eur. Math. Soc., Zürich, 2006.
- [104] Boris Springborn, Peter Schröder, and Ulrich Pinkall. Conformal equivalence of triangle meshes. In *SIGGRAPH '08: ACM SIGGRAPH 2008 papers*, pages 1–11, New York, NY, USA, 2008. ACM.
- [105] Jian Sun, Maks Ovsjanikov, and Leonidas Guibas. A Concise and Provably Informative Multi-Scale Signature Based on Heat Diffusion. In Alexa et al. [22], pages 1383–1392.
- [106] Y. Tong, P. Alliez, D. Cohen-Steiner, and M. Desbrun. Designing quadrangulations with discrete harmonic forms. In Alla Sheffer and Konrad Polthier, editors, *Symposium on Geometry Processing*, pages 201–210, Cagliari, Sardinia, Italy, 2006. Eurographics Association.
- [107] Max Wardetzky. *Discrete Differential Operators on Polyhedral Surfaces - Convergence and Approximation*. PhD thesis, FU Berlin, 2006.
- [108] Henry C. Wente. Counterexample to a conjecture of H. Hopf. *Pacific J. Math.*, 121(1):193–243, 1986.